Pacific Northwest
NATIONAL LABORATORY

PNNL-29186
DVZ-RPT-0027 Rev 0.0

Hanford Surface Barrier Design Guidance

FY19 Status Report

September 2019

Catherine Yonkofski
Z. Fred Zhang

U.S. DEPARTMENT OF ENERGY

Prepared for the U.S. Department of Energy
under Contract DE-AC05-76RL01830

PACIFIC NORTHWEST NATIONAL LABORATORY
operated by
BATTELLE
for the
UNITED STATES DEPARTMENT OF ENERGY
under Contract DE-AC05-76RL01830

Printed in the United States of America

Available to DOE and DOE contractors from the
Office of Scientific and Technical Information,
P.O. Box 62, Oak Ridge, TN 37831-0062;
ph: (865) 576-8401
fax: (865) 576-5728
email: reports@adonis.osti.gov

Available to the public from the National Technical Information Service
5301 Shawnee Rd., Alexandria, VA 22312
ph: (800) 553-NTIS (6847)
email: orders@ntis.gov <https://www.ntis.gov/about>
Online ordering: http://www.ntis.gov

PNNL-29186
DVZ-RPT-0027 Rev 0.0

Hanford Surface Barrier Design Guidance

FY19 Status Report

September 2019

Catherine Yonkofski
Fred Zhang

Prepared for
the U.S. Department of Energy
under Contract DE-AC05-76RL01830

Pacific Northwest National Laboratory
Richland, Washington 99354

Summary

This status report presents results of progress made during fiscal year 2019 towards developing a software tool for designing surface barriers in the Central Plateau. This tool is intended to be used to support feasibility studies and remedy applications. This status report summarizes the methodology followed to develop preliminary vadose zone reduced order models (VZ-ROMs) for use in such a tool.

The ROM development process required generation of a training and testing dataset representing an example waste site in the Central Plateau. This training data was prepared via eSTOMP simulations that simulated variable drainage through hypothetical surface barriers into waste sites within the Central Plateau. Prior to regression analysis, these numerical results were analyzed to understand the behavior of contaminant solutes under different drainage conditions in the vadose zone. Results from eSTOMP simulations provided an understanding of the effectiveness of hypothetical surface barriers in isolating the subsurface system and mitigating contaminant transport.

This first iteration of VZ-ROMs represents the impacts of surface barrier drainage rates on underlying contaminant transport. The preliminary VZ-ROMs developed were specific to the BX-Trenches, and therefore predict impacts to underlying solutes: nitrate (NO_3), technetium-99 (Tc-99), and uranium (U); against two metrics: mass present and plume footprint size for each solute. The resultant combination of six metrics was evaluated for the area directly underlying the evapotranspiration barrier and the area directly underlying the side slopes. A multivariate adaptive regression spline (MARS) model was used to train ROMs to eSTOMP simulations results.

Drainage input parameters for each eSTOMP simulation plot time were provided, and the relationship between the eSTOMP input parameters and the impact metrics were fitted using the MARS implementation. Resultant ROMS predicted total solute mass present over time well as total mass per each unit depth of vadose zone over time. Similarly, the maximum solute footprint over time was predicted along with the solute footprint at each unit depth. Results show preliminary VZ-ROMs fit the simple test data well, and further analysis suggested ways to improve subsequent iterations of ROM parameterization.

The primary objective of the work was to establish an appropriate ROM methodology. Further development is required to adapt the ROMs presented here to appropriately couple surface barrier construction design. Future iterations will be used to predict the performance of different surface barrier engineering designs. Future development will follow a similar process to the one demonstrated in this document.

Acknowledgments

This document was prepared by the Deep Vadose Zone − Applied Field Research Initiative at Pacific Northwest National Laboratory. Funding for this work was provided by the U.S. Department of Energy (DOE) Richland Operations Office. The Pacific Northwest National Laboratory is operated by Battelle Memorial Institute for the DOE under Contract DE-AC05-76RL01830.

Acronyms and Abbreviations

BC	boundary condition
CERCLA	Comprehensive Environmental Response, Compensation, and Liability Act
DOE-RL	U.S. Department of Energy Richland Operations Office
ET	evapotranspiration
GCV	generalized cross-validation
GFM	Geologic Framework Model
MCL	maximum contaminant level
MARS	multivariate adaptive regression splines
MPD	mass per unit depth
NQAP	Nuclear Quality Assurance Program
OLS	ordinary least squares
PHB	Prototype Hanford Barrier
PNNL	Pacific Northwest National Laboratory
RCRA	Resource Conservation and Recovery Act
ROM	reduced order model
SA	surface area
SB-ROM	surface barrier design reduced order model
VZ-ROM	vadose zone reduced order model

Contents

Figures

Tables

1.0 Introduction

Surface barriers (also known as engineered barriers, covers, or caps) have long been considered integral components of final disposal schemes for various types of waste sites throughout the Hanford Site (DOE-RL 1987a,b; 1992a,b,c; 2010). The key functions of a surface barrier are to isolate underlying waste from intrusion and to reduce or eliminate infiltration of water (or drainage) into the waste zone (Fayer et al. 2010). By reducing infiltration into contaminated soil, surface barriers reduce the driving force for downward migration of contaminants. Surface barriers may also reduce migration of windblown contaminated surface soils; penetration of biota into the waste zone; the potential for direct exposure to contamination; and the migration of volatile organic compounds, radon, and tritium to the atmosphere (DOE-RL 2016). The U.S. Department of Energy Richland Operations Office (DOE-RL) specifically identified surface barriers as one of several preferred alternatives that could be applied broadly to contain subsurface contaminants, including deep vadose zone contaminants within the Hanford Site Central Plateau (DOE-RL1987a,b; 1992a,b,c; 2010).

1.1 Surface Barriers at Hanford

Due to the potential broad application of surface barriers, DOE-RL (1987b) recommended that a focused feasibility study be prepared to examine generic surface barrier designs for various waste categories rather than designs for specific waste sites. Subsequently, a multi-year barrier development program was undertaken to develop, test, and evaluate the effectiveness of various barrier designs (DOE-RL 1996). Four barrier designs were developed, each with a set of functional criteria related to the level of protection needed for specific waste sites (DOE-RL 1996; Fayer et. al. 2010). Figure 1 shows cross sections of each design (without side slopes), with layered materials enumerated for reference in the figure. The most protective barrier design was used to build the Prototype Hanford Barrier (PHB). In order of decreasing levels of protection, the remaining three designs are the modified *Resource Conservation and Recovery Act* (RCRA) Subtitle C barrier, the standard RCRA Subtitle C barrier, and the modified RCRA Subtitle D barrier (DOE-RL 1996).

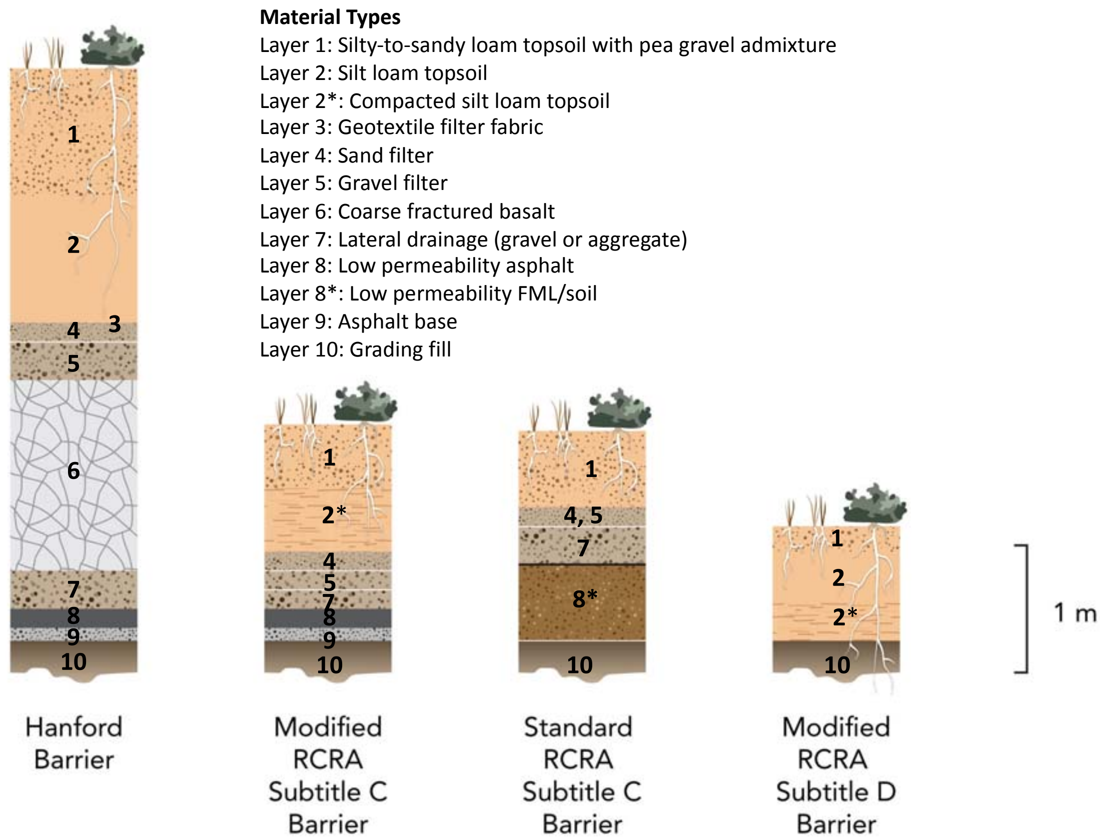

Figure 1. Barrier designs considered in focused feasibility study (after DOE-RL 1996). Individual layers represent different material types, where FML stands for "flexible membrane layer." The depth of plant roots approximates the expected zone of plant water withdrawal. Modified from Fayer et al. (2010).

After a 10-year development period, the Barrier Development Program built the full-scale PHB between late 1993 and 1994 (Wing and Gee 1994) over the 216-B-57 crib in the Central Plateau (DOE-RL 1999). In addition to the layered barrier materials, two side slope designs were incorporated into the final PHB, a 1V:10H sandy gravel side slope and a 1V:3H basalt riprap side slope (Figure 2) (Gee et al. 2002; DOE-RL 2016). The PHB was designed to test a number of design constructs and processes to effectively limit recharge to the subsurface. The following key performance objectives were established (Wing and Gee 1994; DOE-RL 1996, 1999) to address both *Comprehensive Environmental Response, Compensation, and Liability Act* (CERCLA) and RCRA criteria:

- Function in a semiarid to sub-humid climate.
- Have a design life of 1000 years.
- Limit drainage to less than 0.5 mm yr^{-1}.
- Limit runoff.
- Be maintenance free.
- Minimize erosion.
- Meet or exceed RCRA performance criteria.

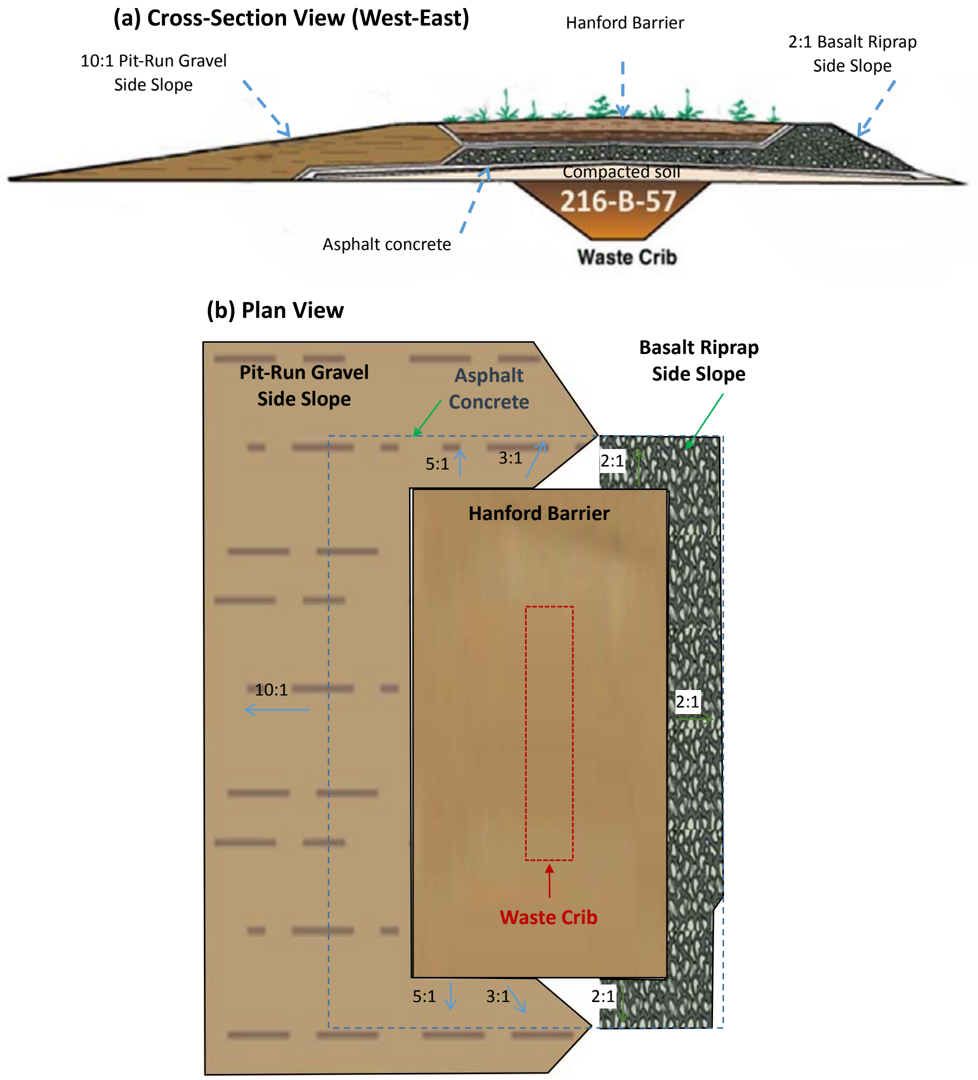

Figure 2. PHB side slope design (a) Cross Section (b) Plan View. After Fig. 2.4 of DOE-RL (2016).

The purpose of the PHB demonstration was to evaluate surface barrier constructability, construction costs, and ecological/hydrologic/structural performance at field scale (DOE-RL 2016). Zhang (2016) presented the hydrology of the PHB's evapotranspiration-capillary barrier from 1994 to 2013, while Zhang (2017) presented the drainage that occurred under two side slopes and evaluated how the drainage from side slopes influences the effectiveness of a long-term barrier. Zhang et al. (2017) described the design solutions and evaluated the performance of the PHB based on monitoring data.

Over the course of a 19-year monitoring period (from 1994 to 2013), the PHB records show the maximum drainage below the barrier was low (0.005 mm yr^{-1}) (DOE-RL, 2016; Zhang 2016). The PHB structure has remained stable through years of wind and water erosion as well as through a controlled burn (Zhang et al. 2017). Overall, the PHB performance objectives were met, with an exception for minimal maintenance required to fill one animal burrow and repair a channel at the foot of the east side slope caused by an unusual runoff event (DOE-RL, 2016; Zhang et al. 2017).

1.2 Needs

The PHB was implemented with the most rigorous design of its time to ensure sufficient safety and functionality; and ultimately, performs much better than the drainage design goal of 0.5 mm yr^{-1} while maintaining structural stability. Retrospectively, the PHB record suggests there may be ways to modify the barrier design to reduce costs yet retain performance. DOE-RL (2016) concluded that analytical and numerical design tools should be developed to support design optimization activities. DOE-RL (2016) specified that tools should account for the impact to performance of changing features such as soil thickness, soil type, and protection from off-site events. Among other things, the tools should be able to address the effective depth (below the barrier) of barrier influence and the integration of surface barriers with other remediation technologies. Finally, the tools should be able to represent (for barrier design purposes) the influence of the topography, hydrology, and proximity to other waste sites that surround a barrier.

1.3 Reduced Order Models

In lieu of field data, which are spatially and temporally limited, computational modeling may be used to estimate the flux of water moving through the vadose zone (Fayer 2000). A number of pre-existing computational tools are available for estimation of water infiltration rate through the vadose zone and, therefore, are applicable to barrier design to varying extents. Most of these approaches rely on water balance models [e.g., the U.S. Environmental Protection Agency's HELP model (Schroeder et al. 1994)] or simulations based on the Richards equation [e.g., UNSAT-H (Fayer 2000) and STOMP (White et al. 2015)]. However, these models can be computationally complex and time consuming, and are not customized to site-specific conditions. Because of the potential broad application of surface barriers to the Central Plateau, efficient, site-specific tools are needed for surface barrier design. Reduced order models (ROMs) may be used as highly efficient surrogates for complex process-based numerical models once trained to a set of numerical model results or observed field data.

Based on the results of numerical models, ROMs use regression analyses to characterize functional relationships from comprehensive suites of physics-based modeled scenarios, often replacing expensive and/or time-consuming runtime computations (when some of the model inputs are varied) with lookup tables, and offering the potential to significantly expedite surface barrier design evaluations. While no ROMs currently exist for surface barrier design, they have been shown to be effective when applied to hydrologic processes (Sharda et al. 2008; Chen et al. 2013, 2014, 2015; Jordan et al. 2015; Keating et al. 2016; Bacon et al. 2019). For example, the MARS (multivariate adaptive regression splines; Friedman 1991) methodology, as implemented in Py-Earth,[1] has recently been used to generate ROMs representative of CO_2 leakage from geologic storage (Keating et al. 2016; Bacon et al. 2019). The ROMs were built for use by stakeholders and output estimates of overlying aquifer impacts due to CO_2 leakage by providing the total volume and dimensions of the impacted aquifer for key monitoring metrics (e.g., changes in pressure, temperature, dissolved CO_2, pH, and total dissolved solids).

[1] https://contrib.scikit-learn.org/py-earth/index.html.

1.4 Scope and Objective

The objective of this effort is to develop a software tool for designing surface barriers in the Central Plateau that can be used to support feasibility studies and remedy applications. The software tool will be provided in a Microsoft Excel Workbook with ROMs and options for flexible user input.

The scope in this first year was to identify barrier impacts within the Central Plateau. Impacts to contaminant migration and distribution were evaluated using eSTOMP-based models that simulated variable drainage through hypothetical surface barriers into waste sites within the Central Plateau. Results shown here focus on the BX-Trenches. Transport and distribution of nitrate (NO_3), technetium-99 (Tc-99), and uranium (U) were recorded over time as a function of drainage. Once a representative set of simulations was generated, results were used to demonstrate a simple example of ROM development specific to the BX-Trenches. From here on, this set of ROMs is referred to as the vadose zone ROMs (VZ-ROMs). These drainage rates, contaminant distributions, and migration rates will be related to specific barrier designs in later years of the task as described in Section 4.1.

This report summarizes the status of this task through fiscal year 2019. Section 2.0 details the methodology followed to generate VZ-ROMs, Section 3.1 summarizes results of preliminary eSTOMP models, Section 3.2 provides an example ROM regression fit to data, and Section 4.0 discusses lessons learned and next steps.

2.0 Methodology

This section describes first describes the BX-Trenches, the physical and hydraulic properties, and other input data needed for the numerical simulations. Then, the simulation scenarios are described, followed by the ROM methodology.

The BX-Trenches consist of eight trenches (Figure 3) and are located southwest of the B-Complex, details of which can be found in Serne et al. (2010). The BX-Trenches were selected for evaluation of surface barrier application within the in the 200 East Area of the Hanford Central Plateau because the main part of the contaminant plumes are currently in the shallow to mid- vadose zone and hence a surface barrier may be effective. The objectives of this simulation study is given below.

1. Establish the current distribution of contaminant. The transport of Tc-99, U, and NO_3 from BX-Trenches was simulated to establish the current (i.e., year 2020) distribution of these contaminants in the vadose zone.

2. Identify the impact of surface barriers on contaminant transport. Barrier impacts were assessed based on changes to the initial spatial (both horizontal and vertical) distribution of contaminants in the vadose zone in year 2020. Flow and contaminant transport was simulated for 100 years (through 2120) under different surface barrier configurations.

3. Create ROMs. The flow and transport simulations were used to train the first iteration of ROMs described in this status report. This demonstrative set of ROMs represent the impacts of surface barrier drainage rates on underlying contaminant transport of the three solutes and two metrics: (1) mass distribution and (2) plume footprint.

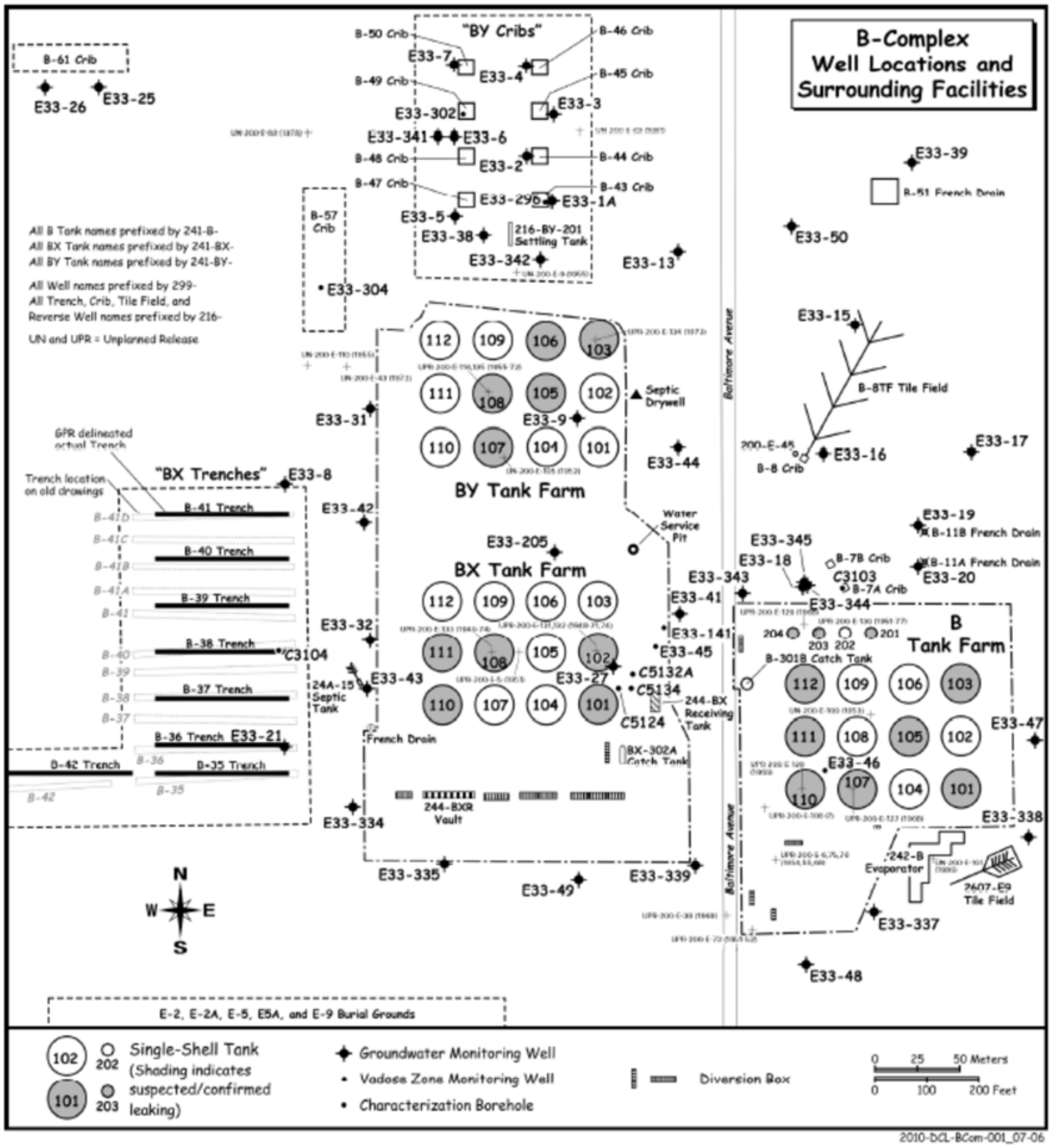

Figure 3. Map of B-Complex Showing Facilities and Key Boreholes and Wells (After Fig. 1.1 of Serne et al. 2010)

2.1 Numerical Simulations

2.1.1 Conceptual Model and Physical Properties

The same geologic conceptual model (Figure 4) described in Rockhold et al. (2018) was used here and is based on the Geologic Framework Model (GFM) for the Central Plateau Vadose Zone described in Springer (2018) and the Hanford South GFM described in Webber (2018). Briefly, the subsurface consisted the following major hydrostratigraphic units from top to bottom:

1. Hanford formation 1 (H1)
2. Hanford formation 2 (H2)

3. Hanford formation 3 (H3)
4. Cold Creek Units (CCUz) that consists of the following sub-units
    a. CCUz-upper silt
    b. CCUz-sand
    c. CCUz-lower silt
5. CCU gravel (CCUg)
6. Ringold Formation that consists of the follow sub-units
    a. Ringold Taylor Flat (Rtf)
    b. Ringold E (Re)
    c. Ringold lower mud (Rlm)
    d. Ringold A (Ra)
7. Basalt (Ba)

The physical, hydraulic and transport parameters for the BX-Trenches are summarized in Table 1, based on data from Last et al. (2006) and Rockhold et al. (2018). In addition, longitudinal and transverse dispersivities were assumed to be 1 m for the Hanford formation through CCU units, and 10 m and 1 m, respectively, for the Ringold formation through basalt (Rockhold et al. 2018). The sorption coefficient (K_d) was zero for Tc-99 and nitrate and 0.1 cm^3g^{-1} was assumed for uranium. It is pointed out that a relatively small k_d value was used based on the observation that the uranium from the BX-102 overfill in 1951 migrated nearly like a conservative solute. The reason for the fast migration of uranium was possibly due to the very large quantity and high concentration of uranium in the leaked fluid. As a result, the sorption capacity of the sand could have been reached and no additional uranium could be sorbed.

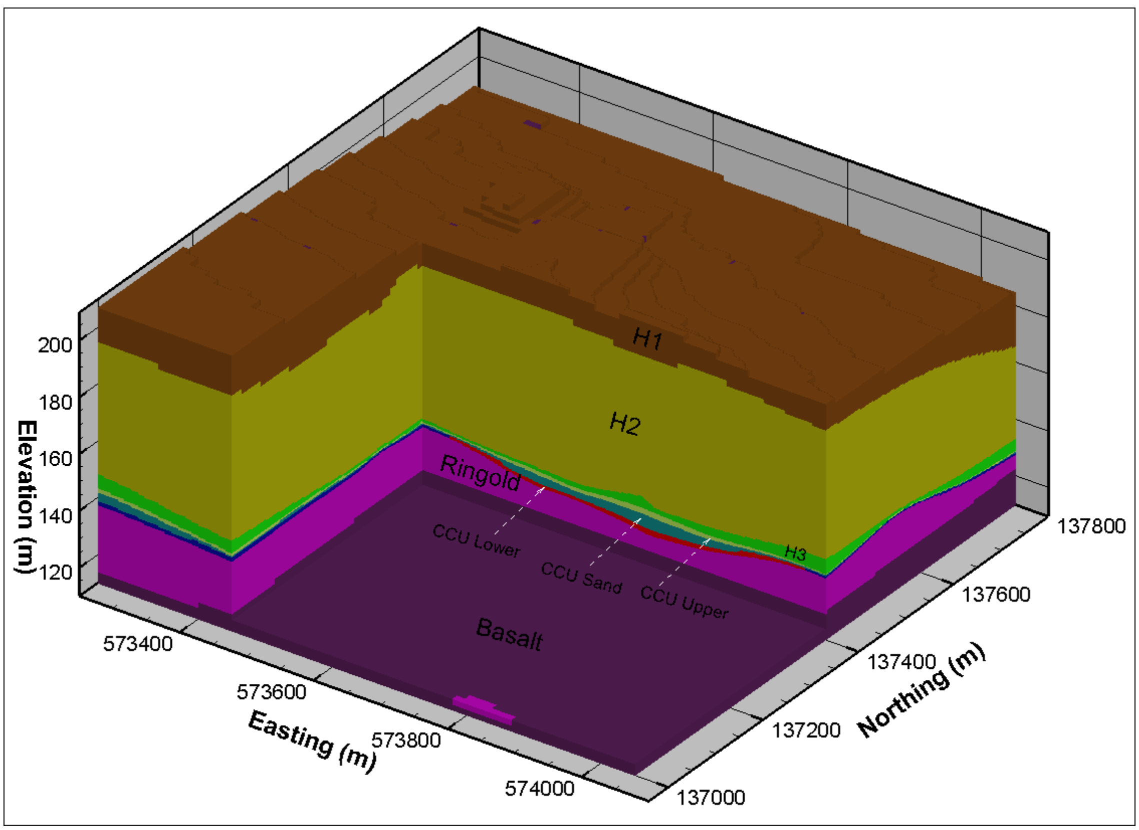

Figure 4. The Rock/soil units below the B-Complex. The silt lenses with the H2 formation are not included.

Table 1. Physical and Hydraulic Parameters Used for Model.

Material	K_{sh} (cm/s)	K_{sv} (cm/s)	K_{sh}/K_{sv}	α (1/cm)	n	S_r	θ_s	θ_{se}	ρ_s (kg/m^3)
Ba	1.62E-08	1.62E-08	1	0.021	1.374	0.0725	0.100	0.080	2720
Ra	1.90E-03	1.90E-04	10	0.0089	1.4739	0.1029	0.379	0.3032	2720
Rlm	3.00E-08	3.00E-08	1	0.0132	1.2586	0.014	0.573	0.4584	2720
Re	4.48E-03	4.48E-03	1	0.0254	2.6566	0.4984	0.221	0.1768	2864
Rtf	6.99E-04	6.99E-05	10	0.0051	3.831	0.4133	0.391	0.3128	2723
CCUg	3.30E-04	3.30E-04	1	0.017	1.73	0.134	0.258	0.2064	2720
CCU_lower	5.57E-05	5.57E-05	1	0.005	2.25	0.097	0.404	0.3232	2820
CCU_sa	1.80E-04	1.80E-04	1	0.0157	1.888	0.123	0.252	0.2016	2820
CCU_upper	5.57E-05	5.57E-05	1	0.005	2.25	0.097	0.404	0.3232	2820
H3	2.66E-03	6.65E-04	4	0.014	2.12	0.14	0.238	0.1904	2720
H2	9.08E-03	2.27E-03	4	0.061	2.03	0.08	0.349	0.2792	2720
H1	2.66E-03	6.65E-04	4	0.014	2.12	0.14	0.238	0.1904	2720
Perchsilt	6.00E-08	6.00E-08	1	0.0046	1.767	0.066	0.376	0.301	2720

Definition of variables:
K_{sh} and K_{sv}: saturated hydraulic conductivity in the horizontal and vertical directions; α: inverse of capillary height; n: a parameter for the Van Genuchten (1980) water retention function; S_r: residual saturation; θ_s: total porosity; θ_{se}: effective porosity; ρ_s: particle density.

2.1.2 Discharge of Fluid and Contaminants

Rockhold et al. (2018, Appendix A.5) compiled the source term information based on Zaher and Agnew (2018). Table 2 tabulates the coordinates that were used to define polygons representing each waste site, the liquid volumes, and mass/activity of NO_3, total uranium (U-total), and Tc-99 that were released to waste sites in the model. All the discharge to the BX-Trenches were in 1953 and 1954.

Table 2. The center of each site and the total release of NO_3, Tc-99, and U-total (Compiled based data in Section A.5 of Rockhold et al. 2018)

		Center of site		Total Release			
Sequence #	Site	x (m)	y (m)	NO_3 [kg]	U-Total [kg]	Tc-99 [Ci]	Liquid Volume (Ml)
1	216-B-35	573430.2	137277.9	114,000	36.3	0.214	1.06
2	216-B-36	573430.2	137293.2	208,000	66.4	0.392	1.94
3	216-B-37	573430.1	137320.6	463,000	148	0.873	4.32
4	216-B-38	573430.0	137348.0	153,000	49	0.289	1.43
5	216-B-39	573429.9	137375.8	165,000	52.7	0.312	1.54

6	216-B-40	573429.8	137402.9	176,000	56.2	0.332	1.64
7	216-B-41	573429.9	137430.1	154,000	49.3	0.291	1.44
8	216-B-42	573338.2	137277.6	298,000	46.5	5.7	1.5
	Sum	N/A	N/A	1,731,000	504.4	8.403	14.87

2.1.3 Initial and Boundary Conditions

The top boundary condition (BC) was the Neumann flux condition defined by the estimated recharge rates (R_w).

- Before the disturbance of the ground surface in 1952, R_w was 2.8 mm yr^{-1}, the average of the estimated value for the primary soils with shrub-steppe vegetation in 200E area (Table 4.15 of Last et al. 2006).
- From 1953 to 1976, R_w was 41.8 mm yr^{-1}, the average of the estimated value for the primary and secondary soils with no vegetation in 200E area.
- From 1977 to 2020, the recharge rate was 5.7 mm yr^{-1}, the average of the estimated value for the primary soils with young shrub-steppe vegetation in 200E area.

The top BCs after 2020 were different for each simulation scenario and are given in section 2.1.5 below. The side BCs were all set as zero-flux and the bottom BC (at the elevation of 122 m) was set a unit gradient. The pre-Hanford subsurface hydraulic condition in 1944 was determined as the steady-state condition under the natural condition (R_w = 2.8 mm yr^{-1}), which was achieved by running the simulation for 10,000 years. It is noted the simulation domain did not include the ground water aquifer. Any mass that left the bottom boundary was considered as the mass to the aquifer. For all the solutes, an outflow boundary condition was used at the bottom.

2.1.4 Pre-Barrier Distribution of Contaminants

In 1953, fluid with dissolved contaminants was discharged to the BX-Trenches. After that, the discharged fluid with dissolved contaminants continued redistributing primarily downward because of gravity. The rate of the infiltration and redistribution and contaminant transport were dependent on a few factors such as the quantity of fluid discharged, the area of the discharge, the sediment properties, and properties of the contaminants.

The year 2020 was selected as the time of surface barrier deployment. The actual distribution of the contaminants at 2020 was unknown. To estimate the pre-barrier contaminant distribution, historical releases of Tc-99, U, and NO_3 from eight sites in the BX-Trenches were simulated from the time of discharge (i.e., 1953) to 2020.

2.1.5 Post-Barrier Flow and Transport

A hypothetical surface barrier was placed over the BX-Trenches in 2020. The surface barrier consisted of an evapotranspiration (ET) barrier, a 12-m-wide side slope, and a 20-m-wide buffer zone (Figure 5). The recharge rates to the subsurface from each of the zones varied (Table 3). For the ET barrier and side slope, three levels (i.e., low, medium, and high) of recharge rates were defined. For the buffer zone, the recharge rate under the natural shrub-steppe vegetation was assumed as given in Table 3. The high value associated with the barrier side slopes was assumed to be twice the average.

Four simulations were conducted corresponding to different surface barrier conditions (Table 4). Case 0 assumed that average vegetation would develop at ground surface and was the control representing recharge rate from the condition of natural vegetation. The three surface barrier cases represented good, average, and poor barrier designs, which were reflected by the low, medium and high recharge rates from the ET barrier and side slope.

Table 3. Definition of drainage rates from the ET barrier and side slope and recharge rates through the buffer zone.

Zone	Value Level	Value (mm yr^{-1})	Description	Notes / Reference
ET Barrier	Low	0	Best-case scenario	
	Medium	0.5	The target rate of a 1000-yr surface barrier	DOE-RL (2016)
	High	4.0	Sparse natural shrub-steppe vegetation	High value in Table 4.15 of Last et al. (2006)
Side Slope	Low	3.0	Average natural shrub-steppe vegetation	Average value for the primary soils in 200 areas. Table 4.15 of Last et al. (2006).
	Medium	23.8	Average rate through the side slopes of PHB from 1994 to 2013 under natural precipitation	Zhang (2017)
	High	47.6	Twice the average	
Buffer Zone	--	3.0	Average natural shrub-steppe vegetation	Average value for the primary soils in 200 areas. Table 4.15 of Last et al. (2006).

Table 4. Definition of simulation cases

Case Number	Surface Barrier Performance	Recharge Level	Recharge Rate (mm/yr)		
			ET Barrier	Side Slope	Buffer Zone and Surrounding Area
0	None	Natural	3.0	3.0	3.0
1	Good	Low	0	3.0	3.0
2	Average	Medium	0.5	23.8	3.0
3	Poor	High	3.0	47.6	3.0

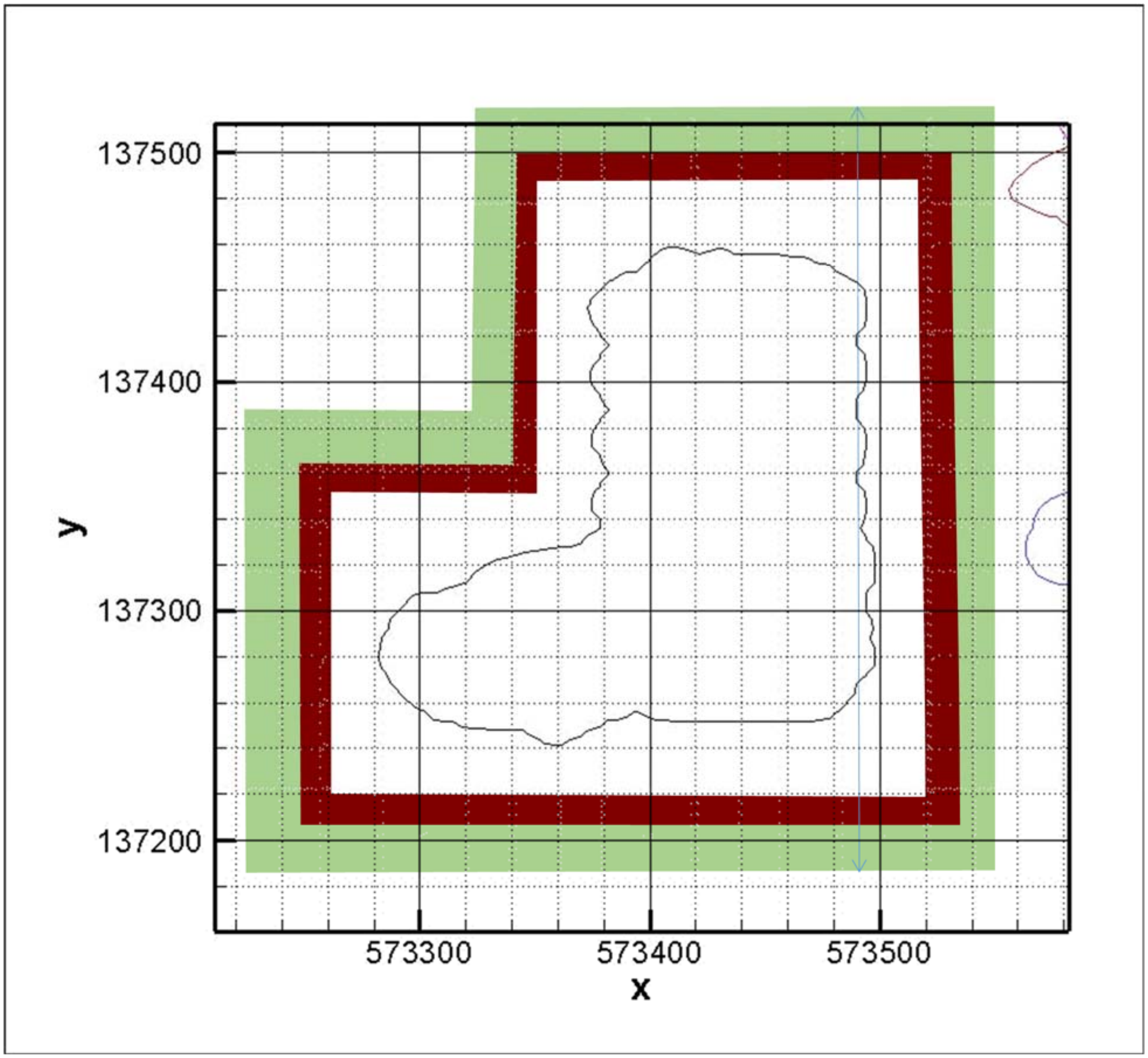

Figure 5. The design of the hypothetical surface barrier over the BX-Trenches. The surface barrier consists of three components: the ET barrier (colored white, in the middle), a 12-m-wide side slope (in brown), and a 20-m-wide buffer zone (in green). The boot-shaped black line shows the boundary of the nitrate plume (in 2020), which is larger than those of technetium and uranium.

2.1.6 Distribution and Extent of Contaminant Plume in the Vadose Zone

The distribution and extent of the contaminants were characterized in a few ways as described below.

Plume Boundary, Areal Extent, Volume, and Mass per Depth

The boundary of a plume is defined as the surface within which the aqueous concentration is equal to or greater than the maximum contaminant level (MCL) for each of the contaminants. The MCLs for the three contaminants of concern in this study are 900 pCi/L for Tc-99[1], 30 µg/L for U-total[2], and 10 mg/L for NO_3[3]. The volume of the plume is the bulk volume within the plume boundary.

The areal extent of a plume is defined as the projection of the plume to a horizontal plane. Its shape is usually irregular, and size is quantified by its area. The vertical distribution of contaminants is characterized by the total mass per unit depth (MPD), which is defined as the total mass of the dissolved contaminant in a given layer divided by the thickness of the layer.

Spatial Moments of a Plume

Spatial moments (M_{ijk}) were used to quantitatively evaluate the changes in the center of mass and its spreading (Aris 1956):

$$M_{ijk}(t) = \int_{x\min}^{x\max}\int_{y\min}^{y\max}\int_{z\min}^{z\max} C(x,y,z,t)x^i y^j x^k dxdydz \tag{1}$$

where C is the concentration per unit bulk volume of sediments; and x_{min}, x_{max}, y_{min}, y_{max}, z_{min}, and z_{max} are the minimum and maximum values of x, y, and z, respectively, of the region, over which the moments are calculated. The zeroth, first, and second spatial moments correspond to $i+j+k =$ 0, 1, and 2, respectively. The zeroth moment (M_{000}) represents the total mass within the region. The normalized first moments, $x_c = M_{100}/M_{000}$, $y_c = M_{010}/M_{000}$, $z_c = M_{001}/M_{000}$, represent the location (x_c, y_c, z_c) of the center of mass. The spread of the contaminant about its center is described by the second moment spatial variance tensor:

$$\begin{gathered}
\sigma^2 = \begin{bmatrix} \sigma_{xx}^2 & \sigma_{xy}^2 & \sigma_{xz}^2 \\ \sigma_{yx}^2 & \sigma_{yy}^2 & \sigma_{yz}^2 \\ \sigma_{zx}^2 & \sigma_{zy}^2 & \sigma_{zz}^2 \end{bmatrix} \\
\sigma_{xx}^2 = \frac{M_{200}}{M_{000}} - x_c^2, \sigma_{yy}^2 = \frac{M_{020}}{M_{000}} - y_c^2, \sigma_{zz}^2 = \frac{M_{002}}{M_{000}} - z_c^2 \\
\sigma_{xy}^2 = \sigma_{yx}^2 = \frac{M_{110}}{M_{000}} - x_c y_c, \sigma_{xz}^2 = \sigma_{zx}^2 = \frac{M_{101}}{M_{000}} - x_c z_c, \sigma_{yz}^2 = \sigma_{zy}^2 = \frac{M_{011}}{M_{000}} - y_c z_c.
\end{gathered} \tag{2}$$

The method may be used in future analysis.

2.1.7 Numerical Simulator

All simulations were carried out using eSTOMP (Fang et al. 2015), the scalable version of the STOMP subsurface flow and reactive transport simulator (White et al. 2015). All simulations were

[1] http://www.iem-inc.com/information/tools/maximum-contaminant-levels-for-water.
[2] https://www.wqa.org/Portals/0/Technical/Technical%20Fact%20Sheets/2014_Uranium.pdf
[3] https://www.epa.gov/ground-water-and-drinking-water/national-primary-drinking-water-regulations.

executed on Constance, a Linux-based cluster that is part of PNNL Research Computing. The eSTOMP simulator is managed as safety software and complies with NQA-1 quality assurance standards.

2.2 Reduced Order Models

Reduced order models are complex regression models fitted to the results of more sophisticated, physics-based numerical simulations. Here, eSTOMP simulations of solute distribution and transport in the vadose zone are fit using Py-Earth[1]. The Py-Earth package is a Python implementation of the Multivariate Adaptive Regression Splines (MARS) algorithm (Friedman, 1991), in the style of scikit-learn[2] (Pedregosa et al. 2011), a library of machine-learning methods written in Python. This section provides an overview of the workflow established to date.

2.2.1 MARS model

MARS is a flexible regression method that automatically searches for interactions and non-linear relationships. A full description of the particular implementation used here may be found in Milborrow (2014); a summary of which is provided below.

Models available in PyEarth may be thought of as linear regression models in a higher dimensional basis space. Each term in an Earth model is a product of hinge functions (or rectifier functions) that are equal to their argument where greater than zero and zero everywhere else (3). An example provided by scikit-learn demonstrates how a simple piecewise linear function in one variable can be expressed as a linear combination of two hinge functions and a constant (4)(Figure 6).

$$h(x-t) = [x-t]_+ = \begin{cases} x-t, & x > t \\ 0, & \leq t \end{cases} \quad (3)$$

Where h(x-t) represents a hinge function.

$$Y = 1 - 2h(1-x) + 12h(x-1) \quad (4)$$

Where the first term is a constant, and the second and third terms are example hinge functions.

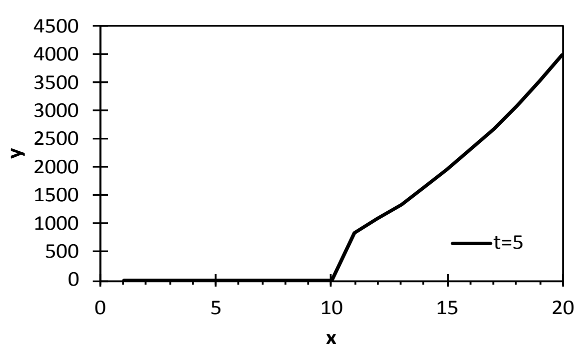

Figure 6. A piecewise linear function as a result of Eqs. (3) and (4).

[1] https://contrib.scikit-learn.org/py-earth/index.html.
[2] http://scikit-learn.org.

During the analysis, the python class, “Earth”, determines which variables and basis functions to use in equation structures like (4). Basis functions may be a constant, an original predictor from the training data set, a hinge function, or a product of two or more hinge functions derived from different predictors. Like standard linear regression, MARS uses the ordinary least squares (OLS) method to estimate the coefficient of each term. However, instead of directly using an original predictor for each term as is done for OLS, each term in a MARS model is a basis function derived from original predictors.

The algorithm has two stages. First, a forward pass searches for terms that locally minimize squared error loss on the training set. Next, a pruning pass selects a subset of those terms that produces a locally minimal generalized cross-validation (GCV) score. The GCV score is not actually based on cross-validation, but rather is meant to approximate a true cross-validation score by penalizing model complexity. The GCV score may be thought of as a prediction score, it is the generalized r^2 of the model on the input and output data. Like an r^2 value, the higher the prediction score the better the fit is. The final result is a nonlinear set of basis functions that are likely to generalize well to predict the trained relationships of interest.

2.2.2 ROM Development

To begin ROM development, domain expertise and/or sensitivity analyses may be used to identify input parameters strongly related to output parameters of interest (i.e., metrics). Numerical simulations are then generated capturing a representative range of values per identified input parameter. These simulation inputs may be parameterized manually or using a more sophisticated method (e.g., Latin hypercube sampling). Typically, the natural system must be simplified to develop a ROM from a numerical simulation training set. These simplifications may be made when the numerical simulations are built or via post-processing techniques. As an example, the physical dimensionality is often reduced from three dimensions to two dimensions or even one dimension

For eSTOMP applications like those shown in this report, 3-D results are simplified into a 2-D representation of data, as formatted in Table 5 for each metric of interest. This is a relatively straightforward process where the 3-D grid is sliced into horizontal layers (e.g., 1-m-thick layers). Lateral heterogeneous distributions are then simplified via averaging or summing, depending on the metric of interest. Then, the relationship between the eSTOMP input parameters and the metrics for each component of interest are fitted using Py-Earth where *x* as exemplified in Eqs. (3) and (4) is set equal to the inputs and *Y* as exemplified in Eq. (4) are the metrics. A similar process is demonstrated in Bacon et al. (2019).

Table 5. Data frame structure data fed to regression analysis.

	Inputs[a]				Outputs[b]		
Simulation #	*Par 1*	…	*Par m*	Time	*Metric 1*	…	*Metric p*
1	<Par (1,1)>	…	< Par (1,m)>	1	<Met (1,1)>	…	<Met (1,p)>
				2	⋮		⋮
⋮	⋮	⋮		⋮			
				<t max>			
<n Sim>	< Par (n,1)>	…	< Par (n,m)>	1	<Met (n,1)>		<Met (n,p)>
				2	⋮		⋮
⋮	⋮	⋮		⋮			
				<t max>			

Where *n* is the number of simulations (Sim), *m* is the number of input parameters (Par), *p* is the number of metrics (Met), and t max is the maximum time.
(a) Input parameters of interest (e.g., horizontal hydraulic conductivity)
(b) Output metrics of interest (e.g., solute mass)

3.0 Results

Prior to regression analysis, numerical results were analyzed to understand the behavior of contaminant solutes in the vadose zone; specifically, NO_3, Tc-99, and U. This section summarizes the results and analysis of eSTOMP simulations and provides example results of ROM development for the BX-Trenches. Detailed eSTOMP simulation results (i.e., training data) are provided in Appendix A and Appendix B.

3.1 eSTOMP Results Summary

Results of the four eSTOMP cases captured the subsurface response to combinations of surface materials with drainage rates representing zero to high recharge values. For this example, the surface materials along with the presence and type of vegetation at the surface determine drainage rates through the barrier, side slope, and surrounding areas (see Section 2.1.5). While more than four cases are recommended to be run for a similar range with refinements to the values of rates tested, these results provided a sufficient characterization for the ROM prototype. Simulation outputs (eSTOMP plot.* files) were recorded once a year for the first 100 years, and again after 200, 500, and 1000 years. The focus on the immediate 100-year time range was chosen as long enough to display significant changes in subsurface solute distributions, and short enough to be computationally efficient for a preliminary demonstration of ROM development.

To process eSTOMP numerical results for use in this demonstration ROM, heterogeneous distributions of solute masses and areal footprints underlying the simulated surface barrier were converted from three dimensions to two dimensions as described in Section 2.2.2. Examples of the processed eSTOMP results comparing solute mass distributions across cases at 100, 500, and 1000 years are shown in Figure 7, Figure 8, and Figure 9.

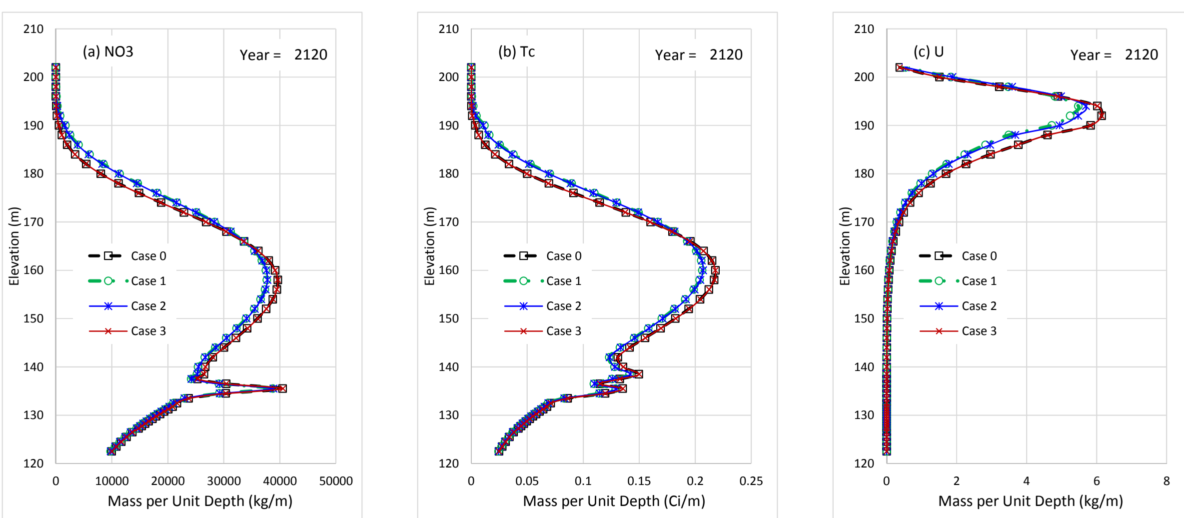

Figure 7. Mass per unit depth at 2120, 100 years after barrier deployment.

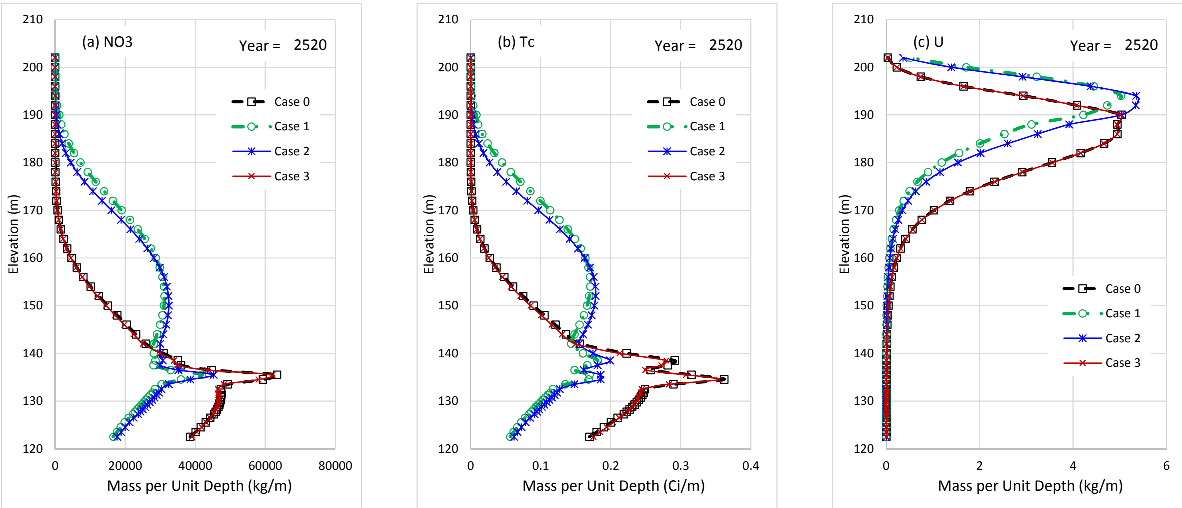

Figure 8. Mass per unit depth at 2520, 500 years after barrier deployment.

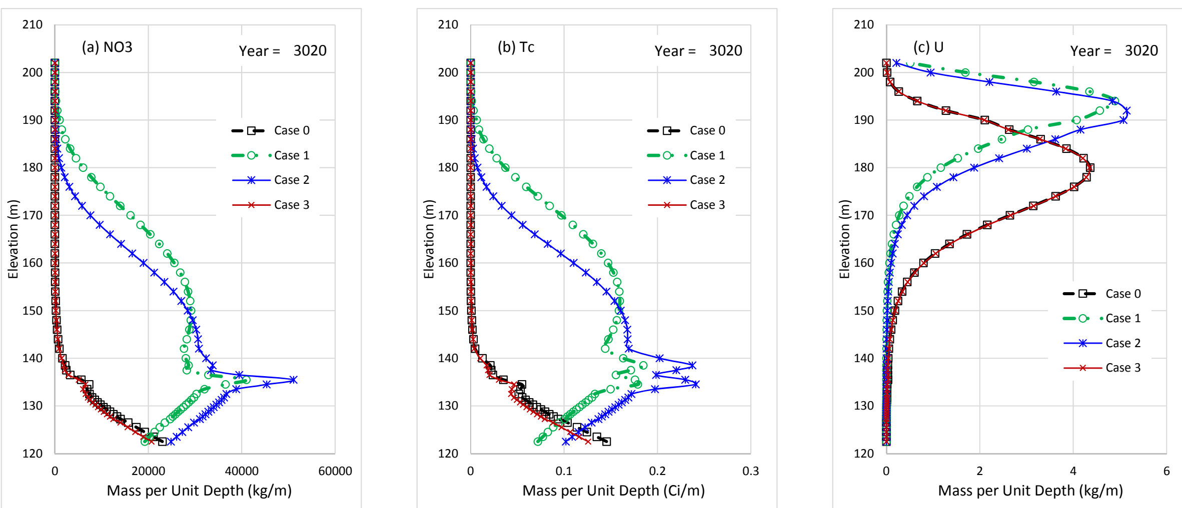

Figure 9. Mass per unit depth at 3020, 1000 years after barrier deployment.

In general, eSTOMP results showed that contaminant migration into groundwater, even under the highest drainage conditions, was quite slow within the first 100 years (detailed results in Section B.2). Once infiltrated, relatively low effective vertical hydraulic conductivity (as compared to aquifers), low initial water content (Appendix A), and a thick depth to groundwater led to these slow recharge conditions. The surface barriers did not impact the water flux to the groundwater until about 25 years post-barrier deployment. Despite the slow response time at depth, more immediate changes were observed within the first 50 m from ground surface.

Drainage in Cases 0 and 3 (no surface barrier, poor surface barrier) led to similar contaminant migration for all solutes at all times. These results indicate that variable drainage through the side slopes was not particularly impactful to contaminant transport in this example; however, more significant differences in contaminant distributions are observed between natural conditions (Case 0) and target conditions (Case 2) of the ET barrier, particularly over long time periods.

3.2 VZ-ROM Development Results

Processed results from eSTOMP simulations were formatted into data frames like Table 6 for each metric (e.g., solute mass, solute surface area). Total drainage volumes were calculated per zone per year up to 100 years. Then, the relationship between drainage volumes per time and the impact metrics for each solute at each unit depth were fitted using Py-Earth. Ultimately, ROMs were generated for each column present under Table 6 "Outputs".

Table 6. Data frame structure for each solute (e.g., NO_3, TC-99, U-total).

Case	Inputs		Time (yr)	Outputs			
	Drainage Vol (m^3)			(Mass, Surface Area)			
	ET Barrier	Side Slope		122.5 m	…	202.5 m	Overall
0	169.4	39.5	1	<MPD, SA>	…	<MPD, SA>	<Total, Max SA>
	⋮	⋮	⋮	⋮		⋮	⋮
1	0	39.5	1				
	⋮	⋮	⋮				
2	28.2	313.0	1				
	⋮	⋮	⋮				
3	169.4	626.0	1				
	⋮	⋮	⋮				

Where MPD is "mass per depth" and SA is "surface area".

Figure 10 and Figure 11 summarize the GCV prediction score for the preliminary VZ-ROM fits specific to the elevations underlying the ET barrier and the side slope respectively. The simulation results closest to the watertable (Near WT) were taken from 122-123 m, middle of the vadose zone (mid VZ) were taken from 162-163 m, and nearest the ground surface (Near GS) were taken from 202-203 m. Results taken over the entire thickness of the vadose zone (Overall) either represented the cumulative masses or the maximum surface area present at any elevation. While there is no set definition for goodness of fit, these prediction scores may be interpreted similar to r^2 values. The backgrounds of these figures represent the increasing goodness of fit as prediction scores approach 1. A negative GCV prediction score can occur and indicates an over-parameterized model — a model that wouldn't generalize well, even though it may be a good fit to the training data. An over-parameterized model is basically interpolating data points. This can occur when there is not enough data or not enough variability in data relative to the number of terms in the ROM. This was the case for NO_3 total mass under the side slope and maximum footprint overall for both NO_3 and Tc-99, plotted with scores of 0 in the figures to demonstrate zero confidence in their predictive ability.

The preliminary BX-Trenches VZ-ROM results should be interpreted with a few notable considerations. As seen in eSTOMP simulation results, the initial U distribution is predominantly near surface. The initial NO_3 and Tc-99 distributions span the entire vadose zone with the bulk of solutes in the mid-vadose zone to near surface. eSTOMP results showed that aqueous flux at depth is not appreciable for a minimum of 25 years post surface barrier implementation, and solute transport in the first 100 years mainly occurs within the shallowest 50 meters depth. Given these conditions, it is expected that the best (i.e., most reliable) predictive capabilities may be near surface for U-total, and mid-vadose zone for NO_3 and Tc-99.

At a glance, it is clear the VZ-ROMs for the area underlying the ET barrier generally tested well all across all metrics, while the VZ-ROMs for the area underlying side slope did not perform as well. However, it is necessary to examine ROM results beyond prediction scores to interpret what aspects of the training set may have contributed to those scores.

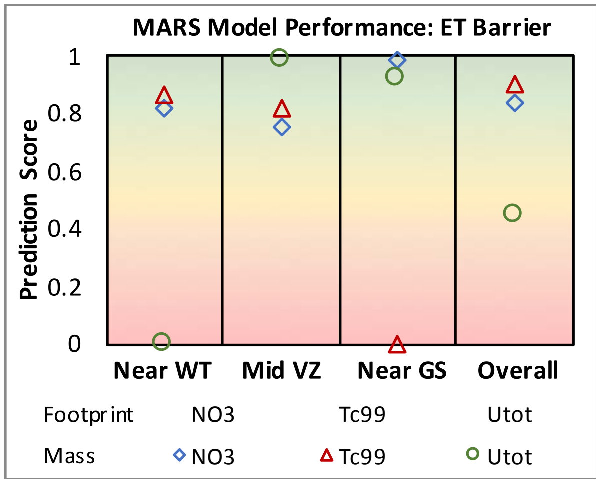

Figure 10. BX-Trenches ET barrier VZ-ROM GCV scores

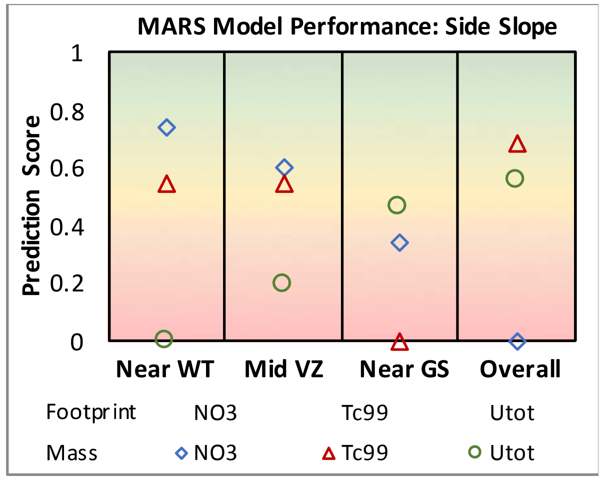

Figure 11. BX-Trenches side slope VZ-ROM GCV scores

3.2.1 VZ-ROM Results per Metric

Panels shown in Figure 12 through Figure 17 display eight plots each. Each plot displays prediction test results which correspond to a GCV prediction score in Figure 10 and Figure 11. eSTOMP simulation results are shown as colored circles (blue for NO3, red for Tc-99, yellow for U) and the VZ-ROM test results are shown as black diamonds. The first and second column of each panel show impact metrics for solutes underlying the ET barrier and the side slope respectively. The first row of panels shows the total mass present in the vadose zone or the maximum surface area throughout the vadose zone, corresponding to “Overall” in Figure 10 and Figure 11. The following rows show metric predictions for solute distributions nearest the watertable, in the middle of the vadose zone, and nearest the surface underlying barrier materials. These panels of plots show a visual depiction of prediction performance for each metric and show generally good prediction capability of the BX-Trenches VZ-ROMs for the expected solutes at elevations defined above. (Note: Vertical axes are set to different scales of best fit per plot).

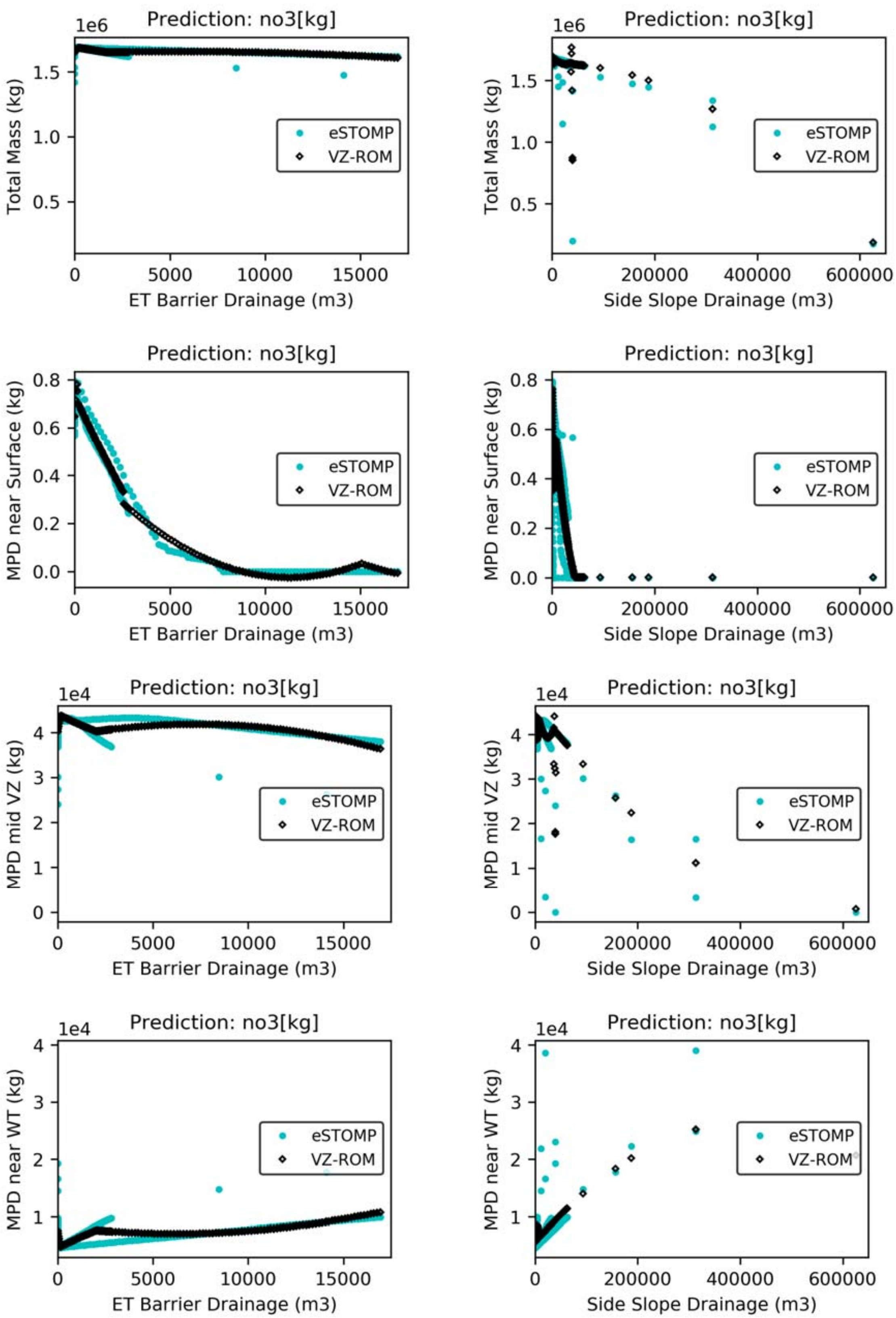

Figure 12. Plots show VZ-ROM test results of NO_3 mass.

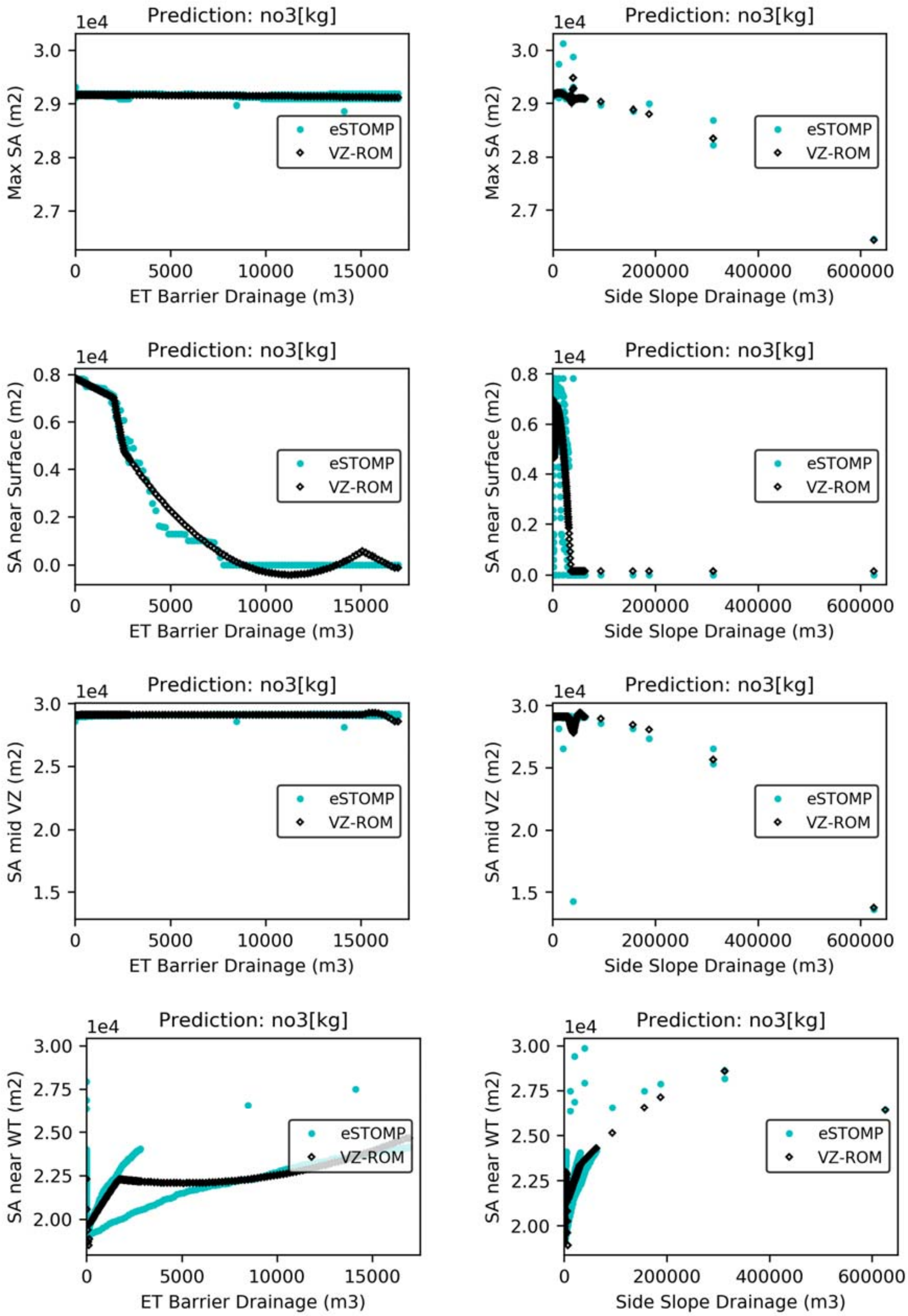

Figure 13. Plots show VZ-ROM test results for the footprint of the NO_3 surface area.

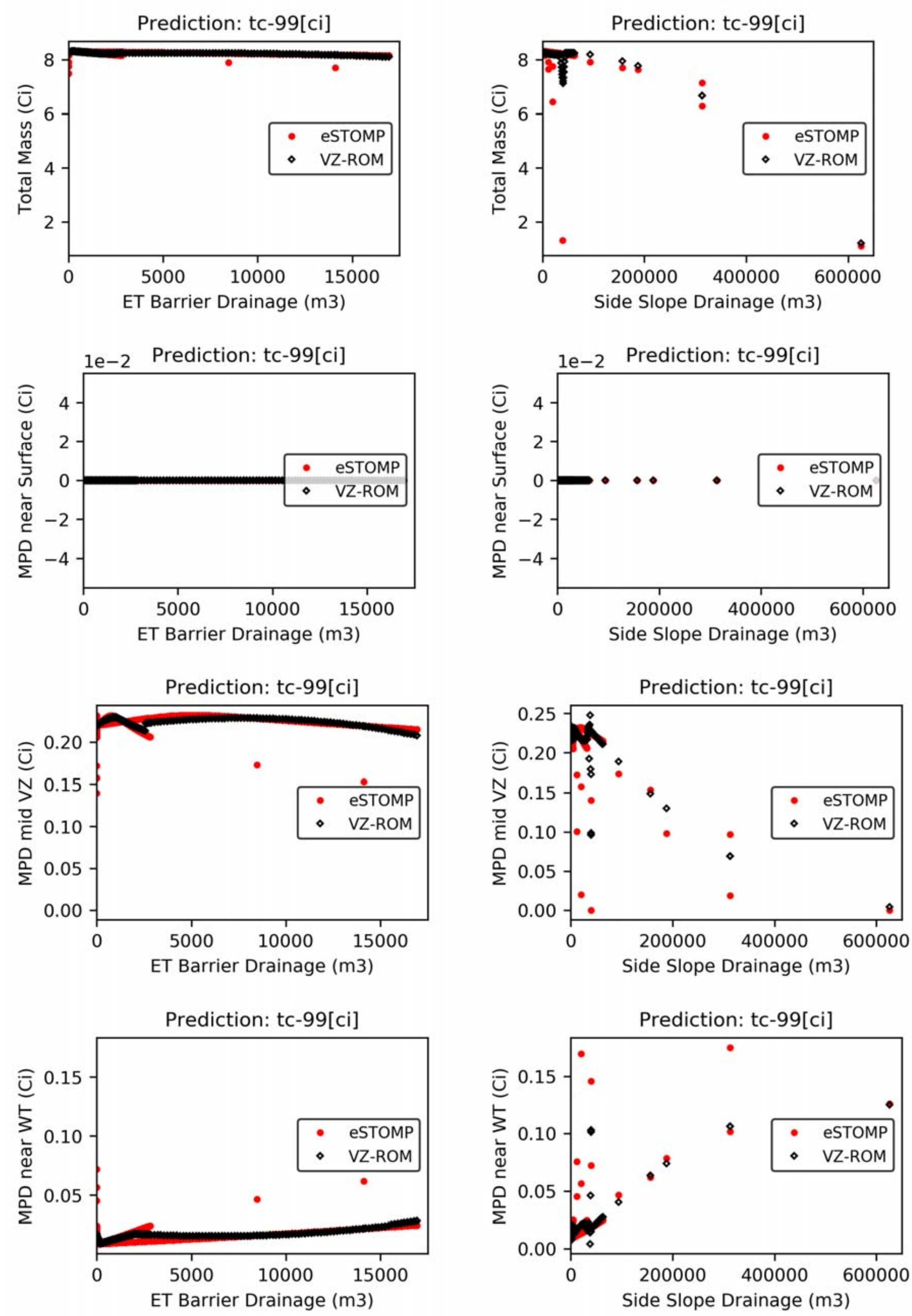

Figure 14. Plots show VZ-ROM test results of Tc-99 mass

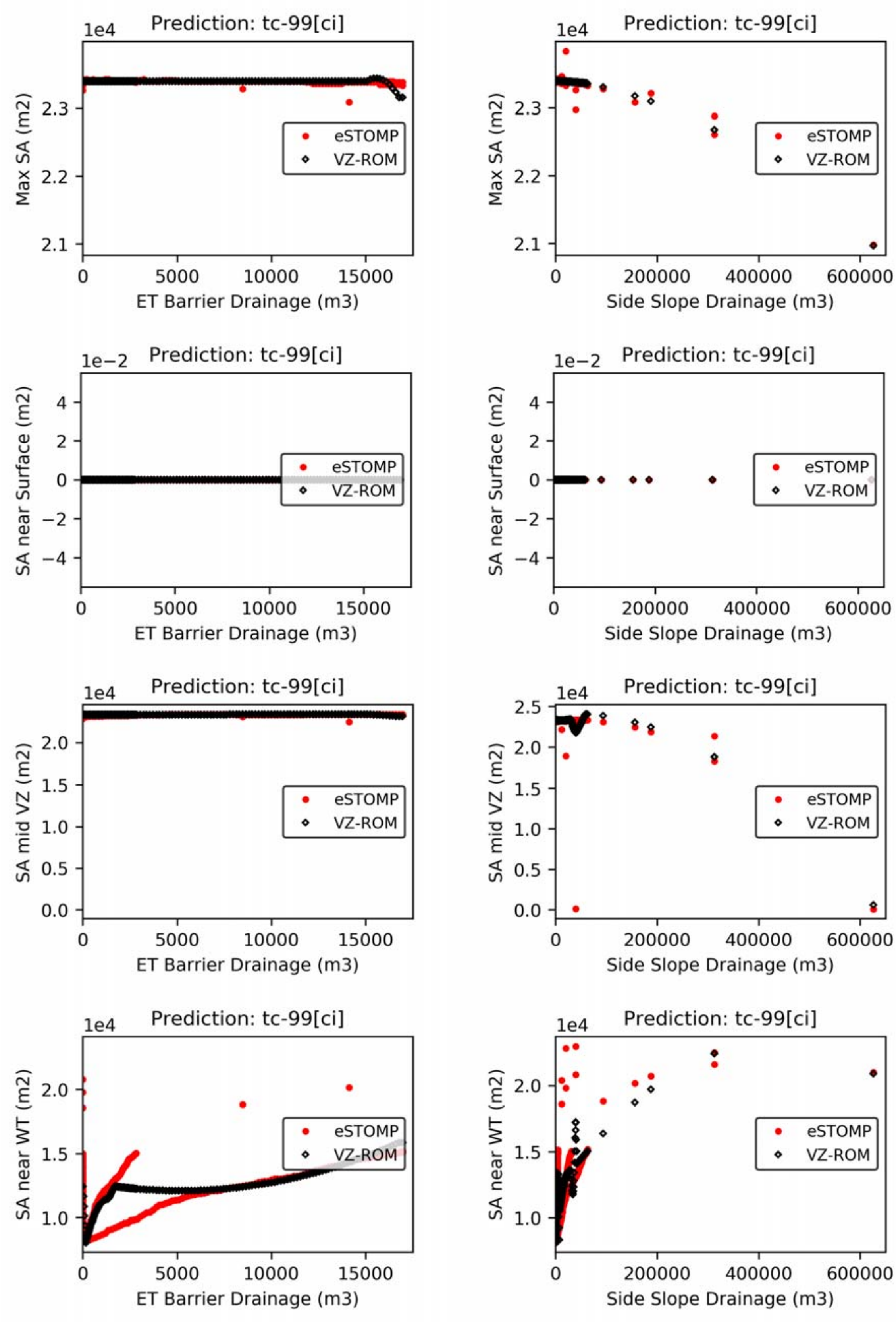

Figure 15. Plots show VZ-ROM test results for the footprint of the T-99 surface area.

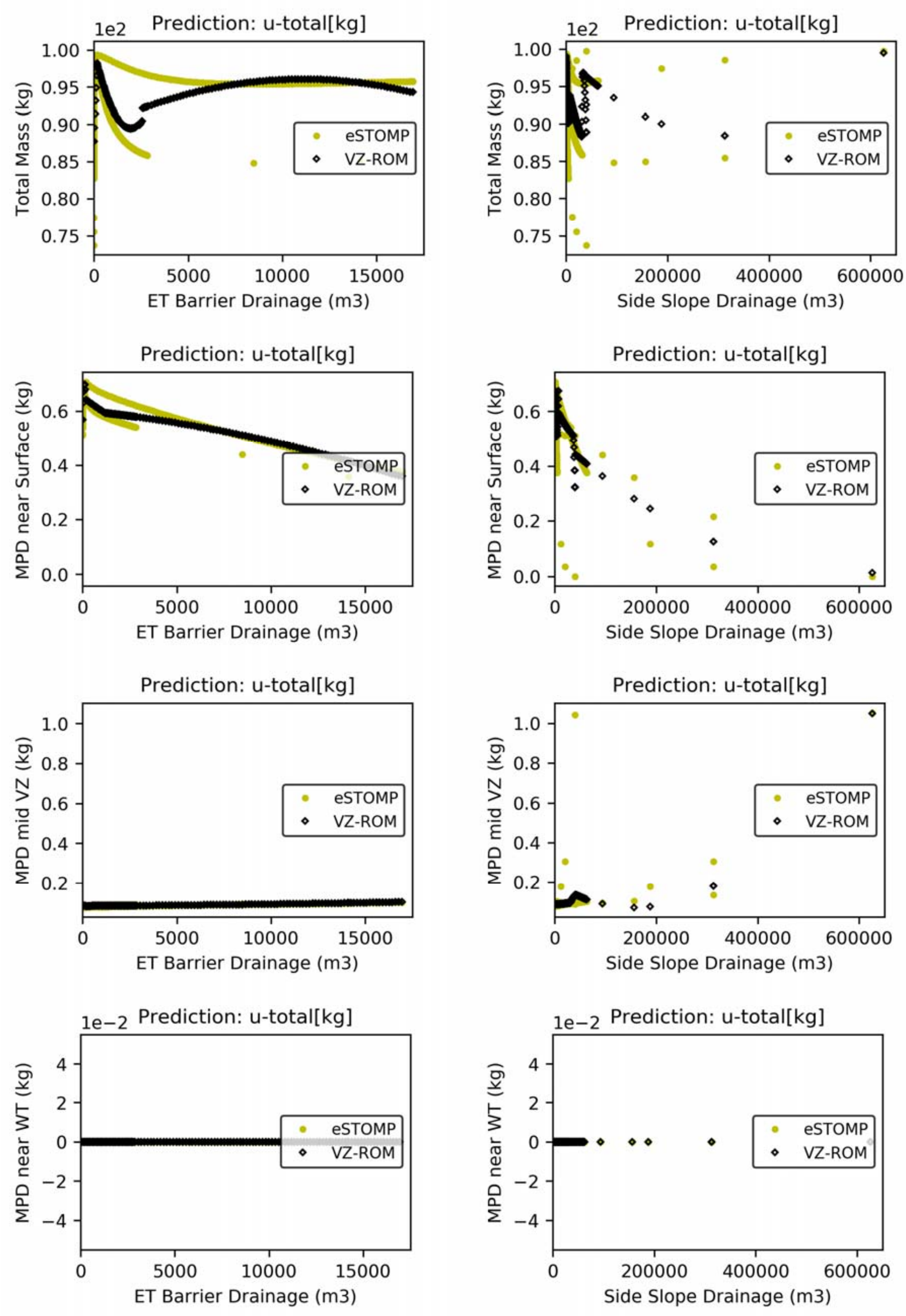

Figure 16. Plots show VZ-ROM test results of U-total mass.

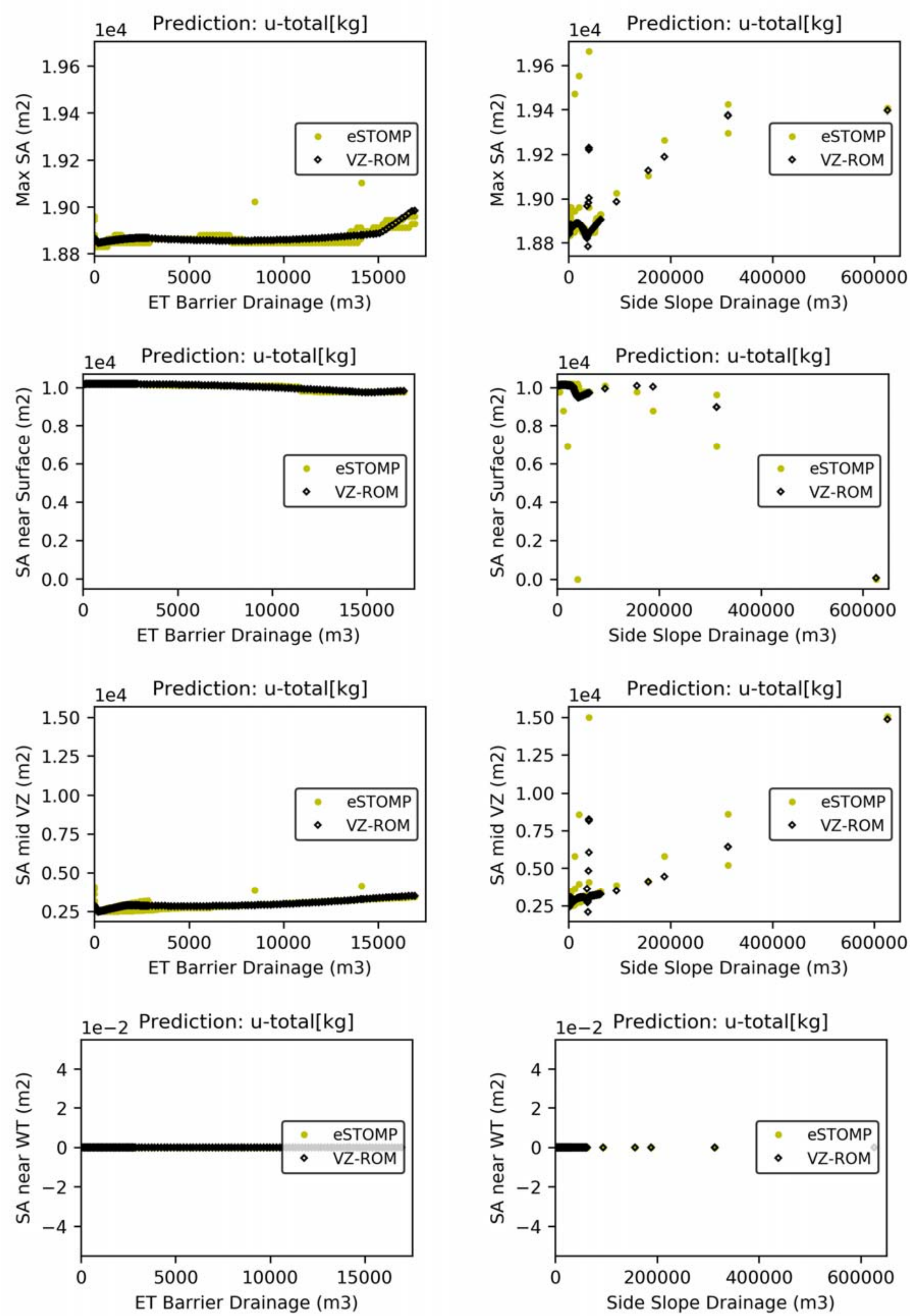

Figure 17. Plots show VZ-ROM test results for the footprint of the U-total surface area.

4.0 Conclusions and Lessons Learned

The preliminary VZ-ROMs developed in this fiscal year demonstrate the methodology for ROM development that will continue to be followed to predict performance of surface barriers in the Central Plateau. This fiscal year, a foundational step was laid in identifying the performance of surface barriers in achieving their purpose: isolation and migration of pre-existing subsurface contaminants. This is also a crucial step in ultimately determining ways to modify the barrier design to reduce costs yet retain performance. Results presented in this status report summarize first steps at meeting DOE-RL needs for analytic and numerical design tools that support surface barrier design optimization activities.

One hundred-year results from eSTOMP simulations provided the training and testing data needed for identifying the effectiveness of surface barriers in isolating the subsurface system and mitigating contaminant transport within the first ~50 m of depth from surface. Due to the simplifications and generalizations required in developing ROMs, output must be interpreted critically. Results suggest a simple improvement to the final software product will be to increase the number of output times from focusing on the first 100 years to considering results for a full 1,000 years.

Based on the significant differences in contaminant distributions observed between natural conditions and target conditions of the ET barrier over long time periods, additional training data are needed to capture drainage rates between 0.5 mm/yr and 3.0 m/yr more thoroughly in these models as well. Other options to improve VZ-ROMs is to vary additional input parameters (e.g., hydrogeologic properties) to obtain additional training data, or to consider mathematical constraints during the development of basis functions for ROMs (maximum number of terms, maximum degree of terms, etc.).

4.1 Next Steps

The VZ-ROM workflow is adaptive so that the complexity can be varied as needed for ROM development. This first iteration of VZ-ROMs represents the impacts of surface barrier drainage rates on underlying contaminant transport. In subsequent work, VZ-ROMs will be coupled to surface barrier design ROMs (SB-ROMs). The software tool will enable rapid assessment of selected barrier design components (e.g., soil thickness, soil type) given site specific considerations (e.g., proximity to other waste sites). Output parameters will include insight into resultant subsurface impacts, costs, and impacts to neighboring waste areas.

To accomplish these goals, additional training datasets will be developed to represent specific barrier components. SB-ROM development will follow a process similar to the one described in this report. A comprehensive ensemble of eSTOMP simulations will be generated to capture the impacts surface barrier engineering decisions on subsurface drainage rates. This ensemble will be used to train SB-ROMs that will provide predicted output as input to the VZ-ROM developed this year. These ROMs will be coded into a spreadsheet tool with a friendly user interface in which users may select from pre-existing barrier designs including the PHB and RCRA barriers described in Section 1.1.1. Users may choose to modify these designs to compare surface barrier performance and estimates of cost. A surface barrier design guidance document will accompany this tool.

5.0 Quality Assurance

This work was performed in accordance with the PNNL Nuclear Quality Assurance Program (NQAP). The NQAP complies with U.S. Department of Energy Order 414.1D, *Quality Assurance,* and 10 CFR 830 Subpart A, *Quality Assurance Requirements*. The NQAP uses NQA-1-2012, *Quality Assurance Requirements for Nuclear Facility Application*, as its consensus standard and NQA-1-2012, Subpart 4.2.1, as the basis for its graded approach to quality.

This work emphasized acquiring new theoretical or experimental knowledge and the initial stages of proving scientific theory. The information associated with this report should not be used as design input or operating parameters without additional qualification.

6.0 References

10 CFR 830, Subpart A. 2011. *Quality Assurance Requirements*. U.S. Code of Federal Regulations.

Aris R. 1956. "On the Dispersion of a Solute in a Fluid Flowing through a Tube." *Proceedings of the Royal Society of London, Series A, Mathematical and Physical Sciences* 235:67-68.

ASME NQA-1-2012, *Quality Assurance Requirements for Nuclear Facility Applications.* American Society of Mechanical Engineers, New York, NY.

Bacon D, C Yonkofski, C Brown, DI Demirkanli, and J Whiting. 2019. "Risk-based Post Injection Site Care and Monitoring for Commercial-Scale Carbon Storage: Reevaluation of the FutureGen 2.0 Site using NRAP-Open-IAM and DREAM." *International Journal of Greenhouse Gas Control (submitted).*

Chen M, Y Sun, P Fu, CR Carrigan, Z Lu, CH Tong, and TA Buscheck. 2013. "Surrogate-based Optimization of Hydraulic Fracturing in Pre-existing Fracture Networks." *Computers & Geosciences* 58:69-79.

Chen M, AF Tompson, RJ Mellors, and O Abdalla. 2015. "An Efficient Optimization of Well Placement and Control for a Geothermal Prospect Under Geological Uncertainty." *Applied Energy* 137:352-363.

DOE Order 414.1D. 2011. *Quality Assurance*. U.S. Department of Energy, Washington, D.C. Approved 4/25/2011.

DOE-RL. 1987a. *Hanford Waste Management Plan*. DOE/RL-87-13. U.S. Department of Energy, Richland Operations Office, Richland, WA.

DOE-RL. 1987b. *Final EIS: Disposal of Hanford Defense High-Level, Transuranic and Tank Wastes*. DOE/EIS-0113, U.S. Department of Energy, Richland Operations Office, Richland, WA.

DOE-RL. 1992a. *200 East Groundwater Aggregate Area Management Study Report*. DOE/RL-92-19, U.S. Department of Energy Richland Operations Office, Richland, WA.

DOE-RL. 1992b. *200 North Aggregate Area Management Study Report*. DOE/RL-92-44, U.S. Department of Energy Richland Operations Office, Richland, WA.

DOE-RL. 1992c. *200 West Groundwater Aggregate Area Management Study Report*, DOE/RL-92-16, U.S. Department of Energy Richland Operations Office, Richland, WA.

DOE-RL. 1996. *Focused Feasibility Study of Engineered Barriers for Waste Management Units in the 200 Areas*. DOE/RL-93-33, Rev. 0, U.S. Department of Energy, Richland Operations Office, Richland, WA.

DOE-RL. 1999. *200-BP-1 Prototype Barrier Treatability Test Report*. DOE/RL-99-11 Rev. 0, U.S. Department of Energy Richland Operations Office, Richland, WA.

DOE-RL. 2010. *Long-Range Deep Vadose Zone Program Plan*. DOE/RL-2010-89 Rev. 0, U.S. Department of Energy Richland Operations Office. Richland, WA.

DOE-RL. 2016. *Prototype Hanford Barrier 1994 to 2015*. DOE/RL-2016-37, Rev. 0, U.S. Department of Energy Richland Operations Office. Richland, WA. Available at https://www.hanford.gov/c.cfm/sgrp/DOE-RL-2016-37/DOE-RL-2016-37_R0.pdf and https://www.hanford.gov/c.cfm/sgrp/DOE-RL-2016-37/Appendices.pdf (Accessed on March 19, 2019).

Fang Y, D Appriou, DH Bacon, VL Freedman, ML Rockhold, CM Ruprecht, GD Tartakovsky, MD White, SK White, and ZF Zhang. 2015. *eSTOMP User Guide*. Accessed on September 27, 2017 at http://stomp.pnnl.gov/user_guide/STOMP_guide.stm (last updated March 2015).

Fayer MJ. 2000. *UNSAT-H version 3.0: Unsaturated Soil Water and Heat Flow Model Theory, User Manual, and Example*, PNNL-13249, Pacific Northwest National Laboratory, Richland, WA.

Fayer MJ, AL Ward, and VL Freedman 2010. *Technical Basis for Evaluating Surface Barriers to Protect Groundwater from Deep Vadose Zone Contamination* PNNL-18661, Pacific Northwest National Laboratory, Richland, WA.

Friedman JH. 1991. “Multivariate Adaptive Regression Splines.” *The Annals of Statistics* 19(1):1-67.

Gee GW, AL Ward, and C Wittreich. 2002. *The Hanford Site 1000-Year Cap Design Test*. PNNL-14143, Pacific Northwest National Laboratory, Richland, WA.

Jordan AB, PH Stauffer, D Harp, JW Carey, and RJ Pawar. 2015. “A Response Surface Model to Predict CO2 and Brine Leakage Along Cemented Wellbores.” *International Journal of Greenhouse Gas Control* 33:27-39.

Keating EH, DH Harp, Z Dai, and RJ Pawar. 2016. “Reduced Order Models for Assessing CO2 impacts in Shallow Unconfined Aquifers.” *International Journal of Greenhouse Gas Control* 46:187-196.

Last GV, GW Gee, EJ Freeman, WE Nichols, KJ Cantrell, BN Bjornstad, MJ Fayer, and DG Horton. 2006. *Vadose Zone Hydrogeology Data Package for Hanford Assessments,* PNNL-14702, Rev. 1, Pacific Northwest National Laboratory. Richland, WA.

Milborrow S, 2014. Notes on the earth package. Retrieved October 31, p. 2017.

Pedregosa F, G Varoquaux, A Gramfort, V Michel, B Thirion, O Grisel, M Blondel, P Prettenhofer, R Weiss, V Dubourg, J Vanderplas, A Passos, D Cournapeau, M Brucher, M Perrot, and É Duchesnay. 2011. “scikit-learn: Machine Learning in Python.” *Journal of Machine Learning Research* 12(2011)2825-2830.

Rockhold ML, X Song, JD Tagestad, PD Thorne, GD Tartakovsky, and X Chen. 2018. *Sensitivity Analysis of Contaminant Transport from Vadose Zone Sources to Groundwater*, PNNL-28065; DVZ-RPT-0015, Rev. 0, Pacific Northwest National Laboratory, Richland, WA.

Schroeder PR, TS Dozier, PA Zappi, BM McEnroe, JW Sjostrom, and RL Peyton. 1994. *The Hydrologic Evaluation of Landfill Performance (HELP) Model: Engineering Documentation for Version 3.* EPA/600/R-94/168b, U.S. Environmental Protection Agency, Risk Reduction Engineering Laboratory, Cincinnati, OH.

Serne RJ, BN Bjornstad, JM Keller, PD Thorne, DC Lanigan, JN Christensen, and GS Thomas. 2010. *Conceptual Models for Migration of Key Groundwater Contaminants through the Vadose Zone and into the Unconfined Aquifer Below the B-Complex*. PNNL-19277, Pacific Northwest National Laboratory. Richland, WA.

Sharda VN, SO Prasher, RM Patel, PR Ojasvi, and C Prakash. 2008. “Performance of Multivariate Adaptive Regression Splines (MARS) in predicting runoff in mid-Himalayan micro-watersheds with limited data” / “Performances de régressions par splines multiples et adaptives (MARS) pour la prévision d'écoulement au sein de micro-bassins versants Himalayens d'altitudes intermédiaires avec peu de données.” *Hydrological Sciences Journal* 53(6):1165-1175.

Springer SD. 2018. *Model Package Report: Central Plateau Vadose Zone Geoframework*. CP-60925, Rev. 0, CH2M Hill Plateau Remediation Company, Richland, WA.

Van Genuchten MT. 1980. “A Closed-Form Equation for Predicting the Hydraulic Conductivity of Unsaturated Soils.” *Soil Science Society of America Journal* 44:892-898.

Webber MC. 2018. *Development of the Hanford South Geologic Framework Model, Hanford Site, Washington*. ECF-HANFORD-13-0029, Rev. 5, CH2M Hill Plateau Remediation Company, Richland, WA.

White MD, D Appriou, DH Bacon, Y Fang, VL Freedman, ML Rockhold, CM Ruprecht, GD Tartakovsky, SK White, and ZF Zhang. 2015. *STOMP/eSTOMP User Guide*. PNNL-SA-108766, Pacific Northwest National Laboratory, Richland, WA. Accessed on October 29, 2015, at http://stomp.pnnl.gov/user_guide/STOMP_guide.stm (last updated March 2015).

Wing NR and GW Gee. 1994. “Quest for the Perfect Cap.” *Civil Engineering* 64(10):38-41.

Zaher U and S Anew. 2018. *Hanford Soil Inventory Model (Sim-V2) Calculated Radionuclide Inventory of Direct Liquid Discharges to Soil in the Hanford Site's 200 Areas*. ECF-HANFORD-17-0079, CH2M Hill Plateau Remediation Company, Richland, WA.

Zhang ZF, CE Strickland, and SO Link. 2017. “Design and Performance Evaluation of a 1000-Year Evapotranspiration-Capillary Surface Barrier.” *Journal of Environmental Management* 187:31-42.

Zhang ZF. 2016. “Long-Term Hydrological Characteristics of an Evapotranspiration-Capillary Barrier for Infiltration Control and Waste Isolation.” *Water Resources Research* 52:4883-4904. doi:10.1002/2015WR018167.

Zhang ZF. 2017. “Long-Term Drainage from the Riprap Side Slope of a Surface Barrier.” *Water* 8:156-164.

Appendix A: Pre-barrier Distribution of Water and Contaminants

The contaminated water was discharged to the BX-Trenches in 1953 and 1954. The simulated distributions of soil moisture in 1955 (right after fluid discharge) and 2020 (before barrier deployment) are shown in Figure A.1. In 1955, the discharged fluid caused higher water content zones as shown by the red color in Figure A.1(a). The discharged water arrived at the ground water at about 1962. By 2020, as shown by Figure A.1(b), the higher water content zone had disappeared, indicating most of the discharged water had left the vadose zone and reached the groundwater.

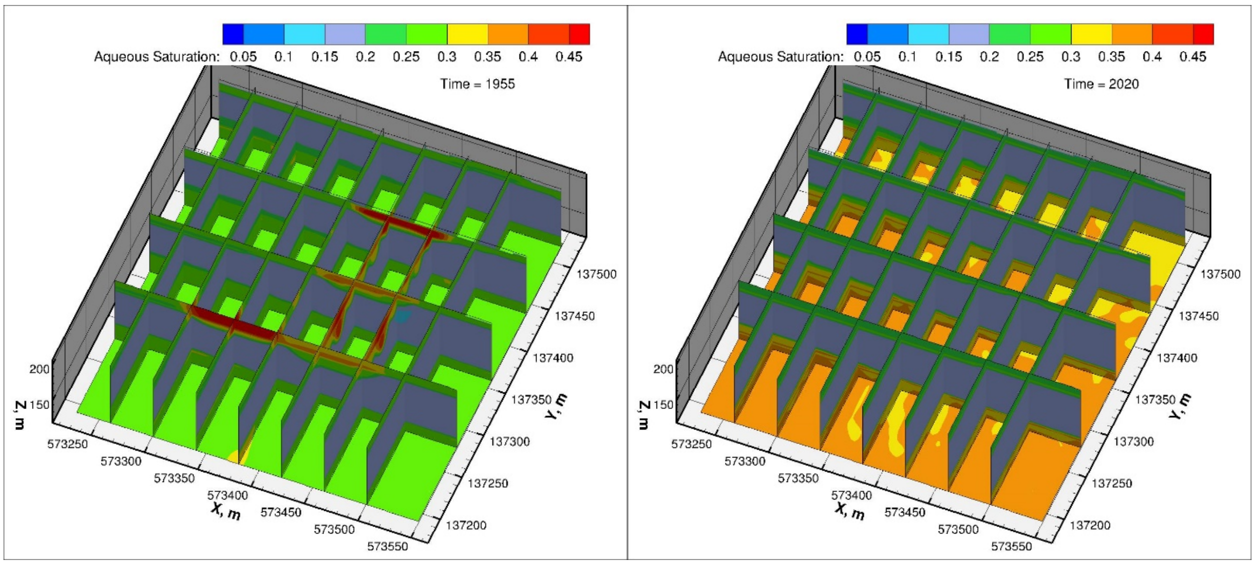

(a) 1955 (b) 2020

Figure A.1. The aqueous saturation in 1955 (right after the discharge in 1954) and in 2020 (right before the deployment of the hypothetical barrier)

The simulated distributions of NO_3, Tc-99, and U-total in 1955 and 2020 are shown in Figure A.2, Figure A.3, and Figure A.4, respectively. The contaminant concentrations are shown on multiple vertical and one horizontal slices to reveal the three-dimensional plume below the ground surface, especially below the BX-trenches. The MPD curves of the three contaminants from 1955 to 2020 are shown in Figure A.5. The fraction of discharged contaminant mass retained in the vadose zone is shown in Figure A.6. Different from water, most of which had entered the groundwater by 2020, at least 97.6% of the contaminants had not reached the groundwater although NO_3 and Tc-99 were not sorbed by the sediments. The reason for slower migration of contaminants was due to the existence of residual water, which can dissolve contaminants but is immobile. The residual water is the water resides in the smallest pores that may be disconnected each other. As a result, the residual water is generally immobile. The mobile water flows much faster than the average contaminant plumes. The U-total plume was shallower than NO_3 and Tc-99 because U adsorbed to sediments. Figure A.7 shows the pre-barrier extents of the three contaminants in the horizontal plane. The three plumes had similar shapes, as expected, while the NO_3 plume was slightly larger than the Tc-99 plume, which was slightly larger than the U-total plume.

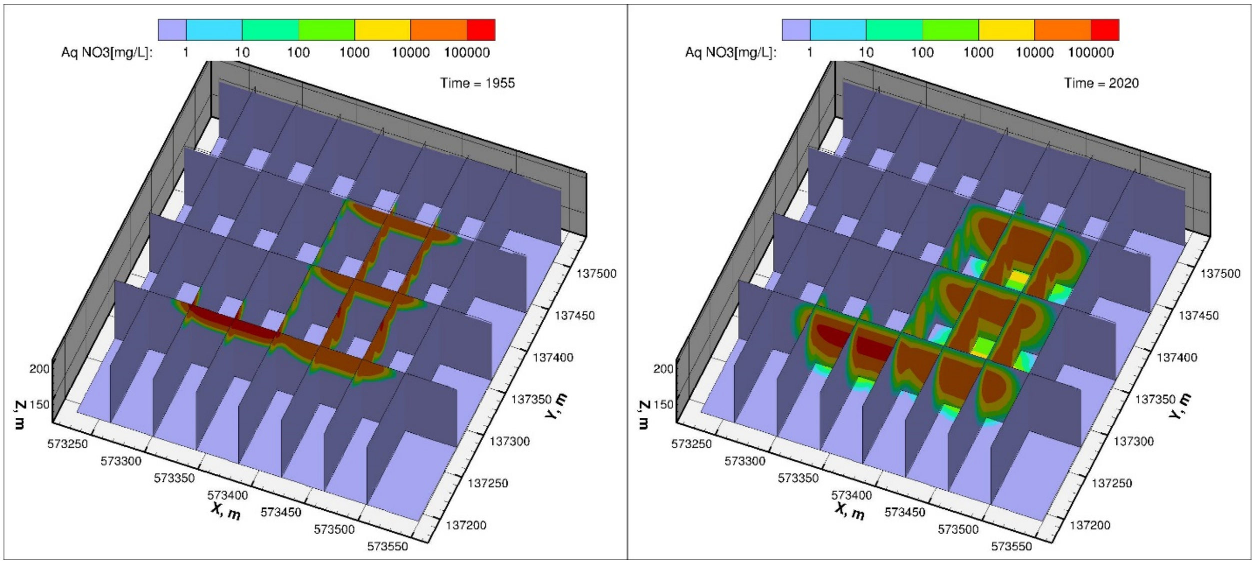

(a) 1955 (b) 2020

Figure A.2. The nitrate concentration in 1955 (right after the discharge in 1954) and in 2020 (right before the deployment of the hypothetical barrier).

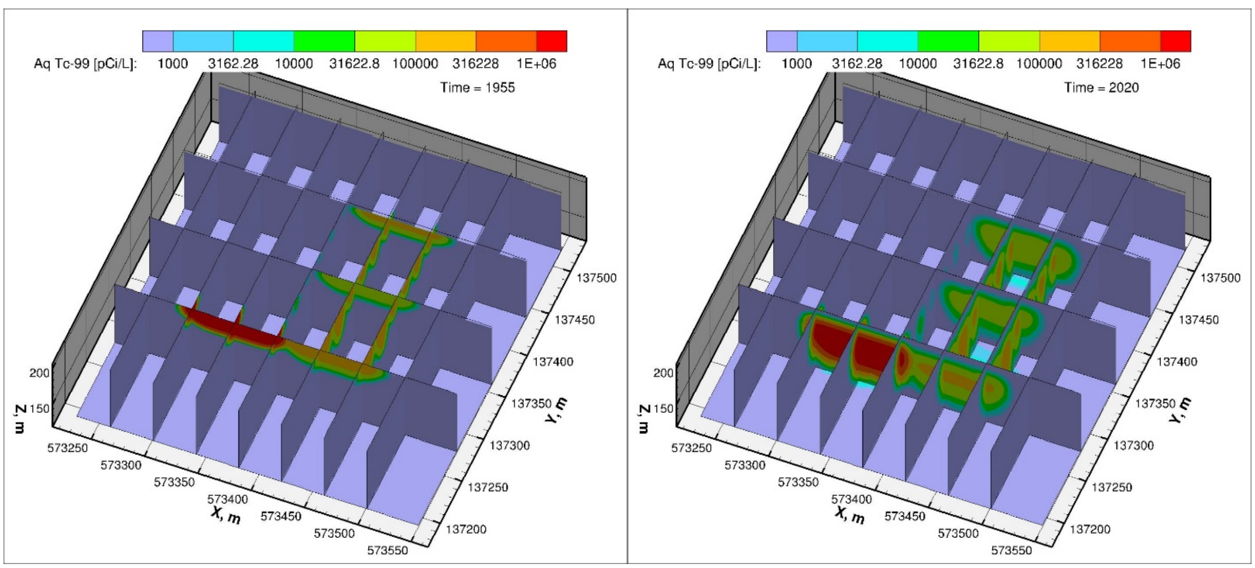

(a) 1955 (b) 2020

Figure A.3. The Tc-99 concentration in 1955 (right after the discharge in 1954) and in 2020 (right before the deployment of the hypothetical barrier).

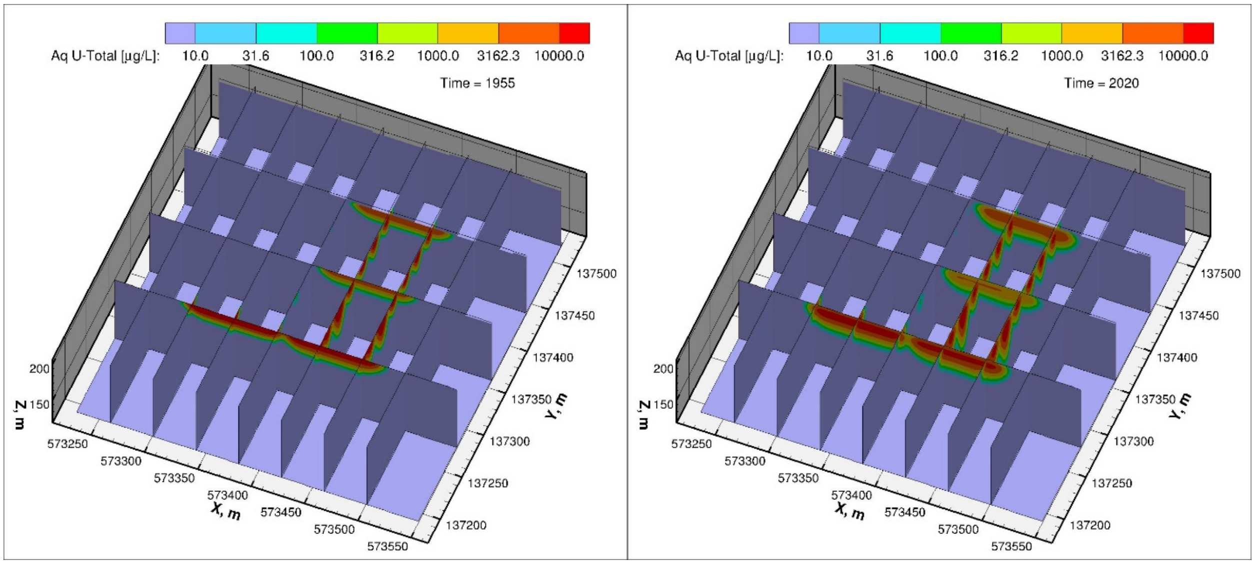

(a) 1955 (b) 2020

Figure A.4. The uranium concentration in 1955 (right after the discharge in 1954) and in 2020 (right before the deployment of the hypothetical barrier). The sorption coefficient was assumed to be 0.1 $cm^3\ g^{-1}$.

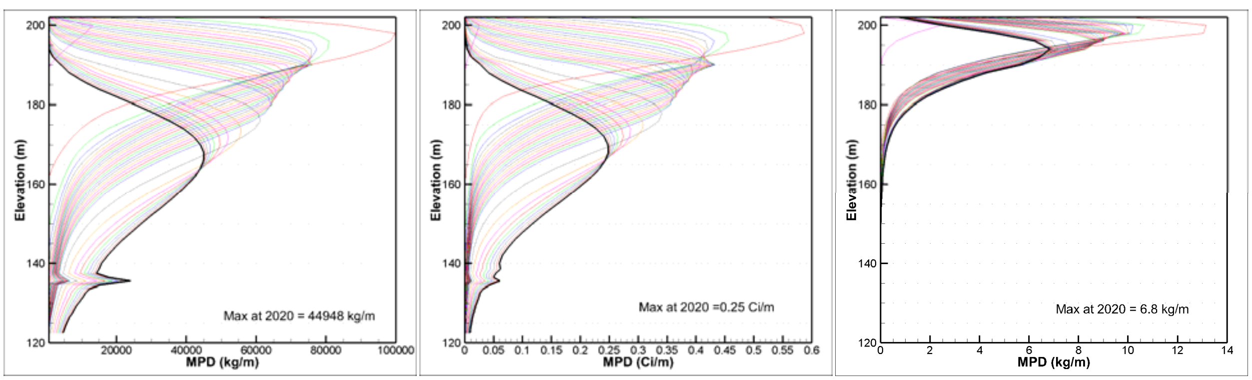

(a) NO_3 (b) Tc-99 (c) U (aqueous)

Figure A.5. MPD from 1954 to 2020. The thick black lines correspond to the PMD in 2020.

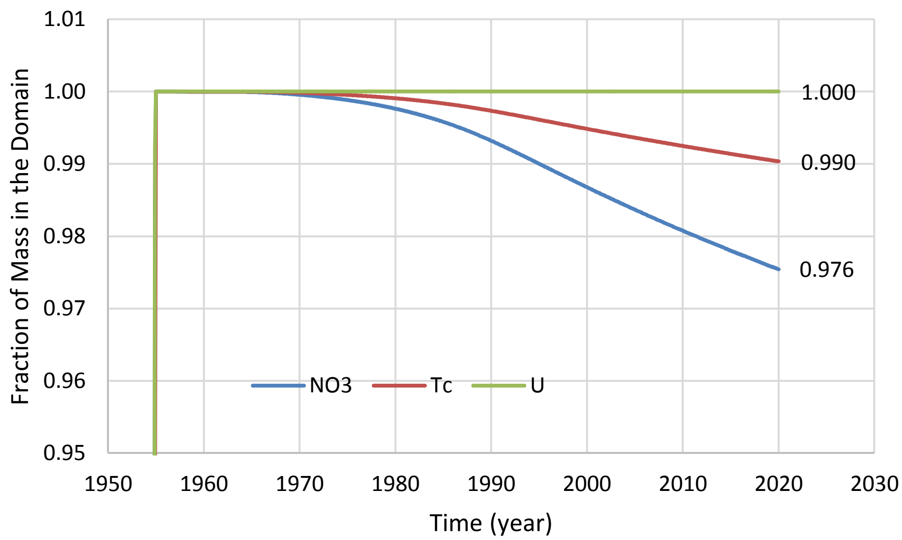

Figure A.6. Fraction of the discharged mass retained in the domain.

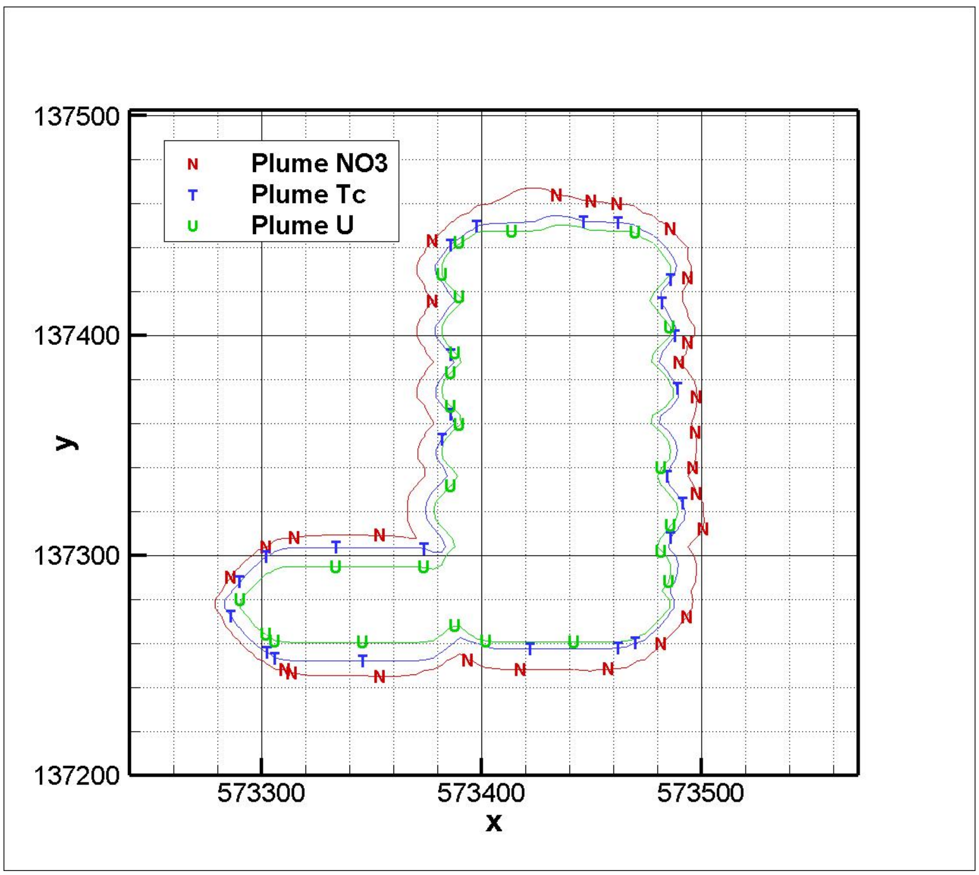

Figure A.7. Pre-barrier (at 2020) plume extent at the horizontal plane. The boundaries of each plume correspond to the maximum contaminant level (MCL) of each contaminant. The MCLs are 1 mg L^{-1} for NO_3, 900 pCi L^{-1} for Tc-99, and 30 μg L^{-1} for U.

Appendix B: Post-barrier Contaminant Transport

The water flow and contaminant transport after barrier deployment in 2020 are presented below for the four cases described in Table 4 of the main report: Case 0 (no surface barrier), Case 1 (good performing surface barrier), Case 2 (average performing surface barrier), and Case 3 (poor performing surface barrier) .

B.1 Aqueous Saturation

Figure B.1 demonstrates the aqueous saturation at 2120, 100 years after surface barrier deployment, for the four simulation cases. Roughly, the saturation distribution for Case 0 (no surface barrier) is similar to Case 3 (poor surface barrier), while the saturation distribution for Case 2 (good surface barrier) is similar to Case 3 (average surface barrier). However, the poor surface barrier (Case 3) is wetter than the no surface barrier (Case 0) below the side slope area, which is shown by the orange color at the horizontal plane in Figure B.1d. This is because the side slope of the surface barrier enhanced precipitation recharge. Under a good surface barrier (Case 1) or an average surface barrier (Case 2), a relatively drier zone can be seen in the zone below the evapotranspiration (ET) surface barrier.

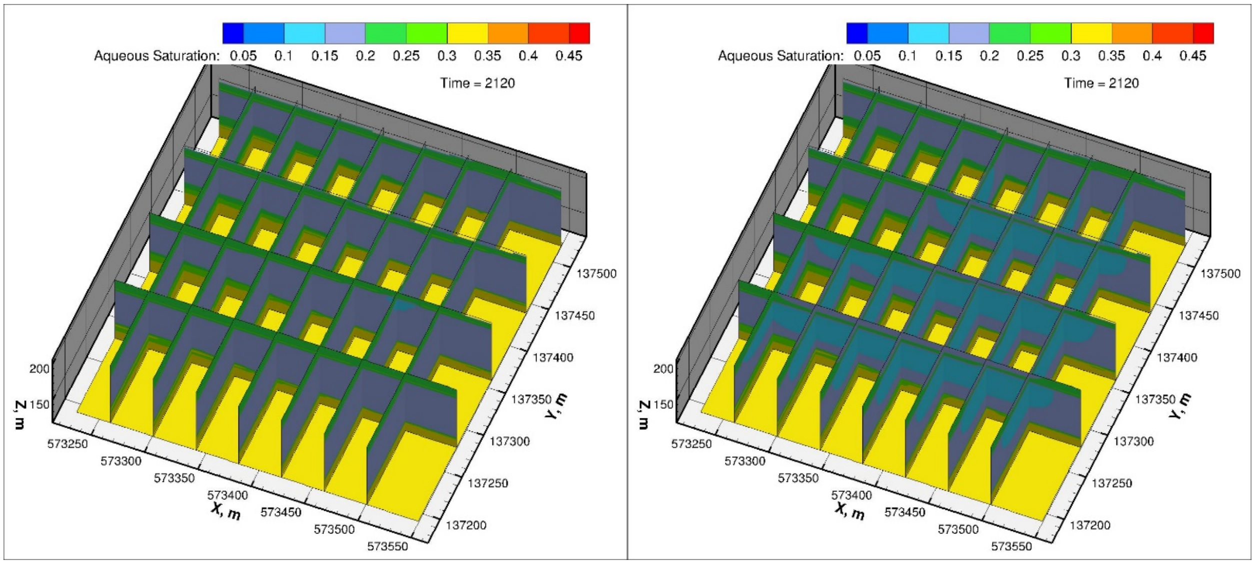

(a) Case 0 (No surface barrier) (b) Case 1 (Good surface barrier)

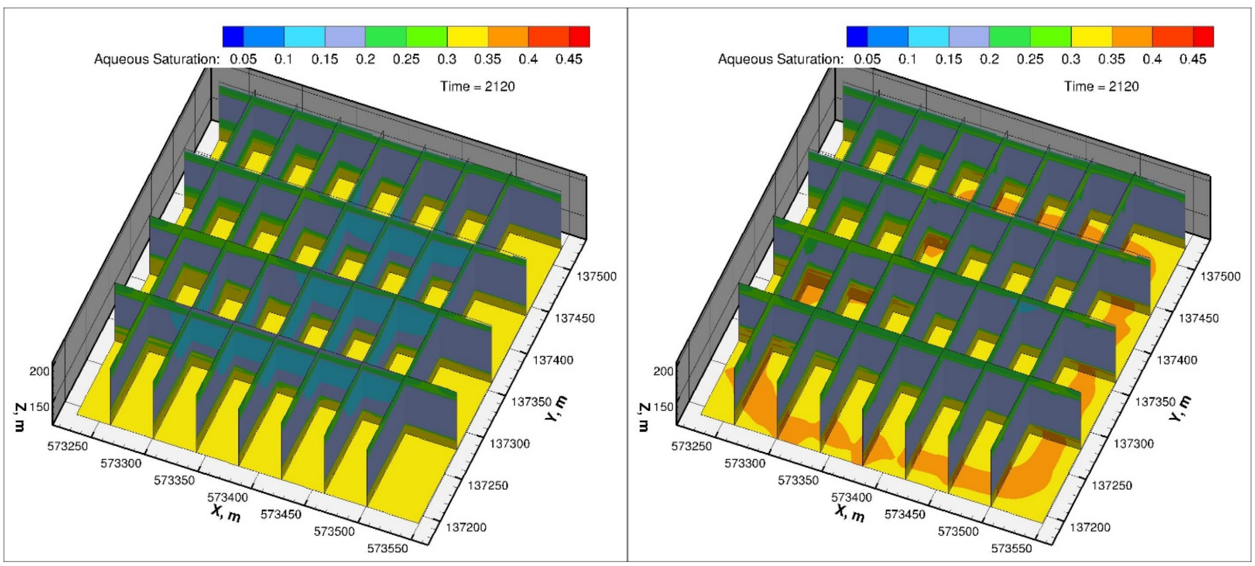

(c) Case 2 (Average surface barrier) (d) Case 3 (Poor surface barrier)

Figure B.1. Aqueous saturation at 2120, 100 years after surface barrier deployment.

B.2 Aqueous Flux Rates at GW Table

Figure B.2 depicts the aqueous flux rates from the ET barrier, the side slope, and the buffer zones to the groundwater for the simulation cases. For the first 25 years since surface barrier deployment (Δt), the flux rates to the groundwater in all the zones for all the cases were the same, indicating the surface barrier did not have any impact on the water flux to the groundwater during this period. After approximately 50 to 200 years of transition, the flux rates approached a steady-state value. However, the flux rates from the ET barrier zone for the three cases with barriers (0.6, 2.5, and 6.5 mm yr^{-1} for Cases 1, 2, and 3, respectively) never equilibrated to the surface barrier rate (i.e., 0, 0.5, and 3.0 mm yr^{1} for Cases 1, 2, and

3, respectively) even after 1000 years because of a fraction of water migrated from the wet zone below the side slope to the zone beneath the ET barrier.

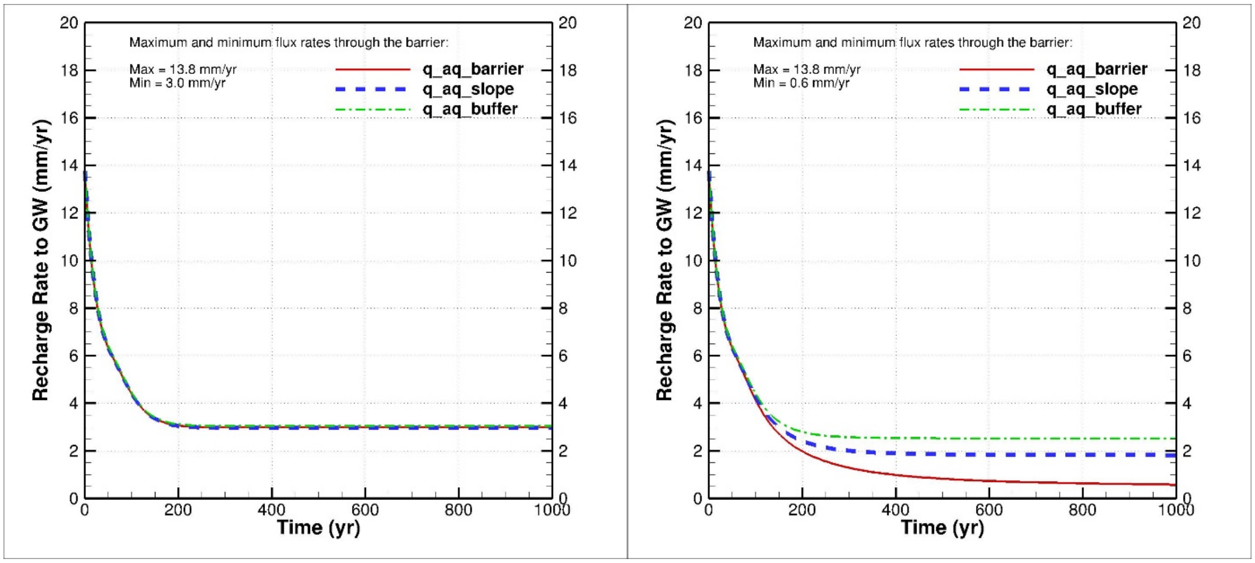

(a) Case 0 (No surface barrier) (b) Case 1 (Good surface barrier)

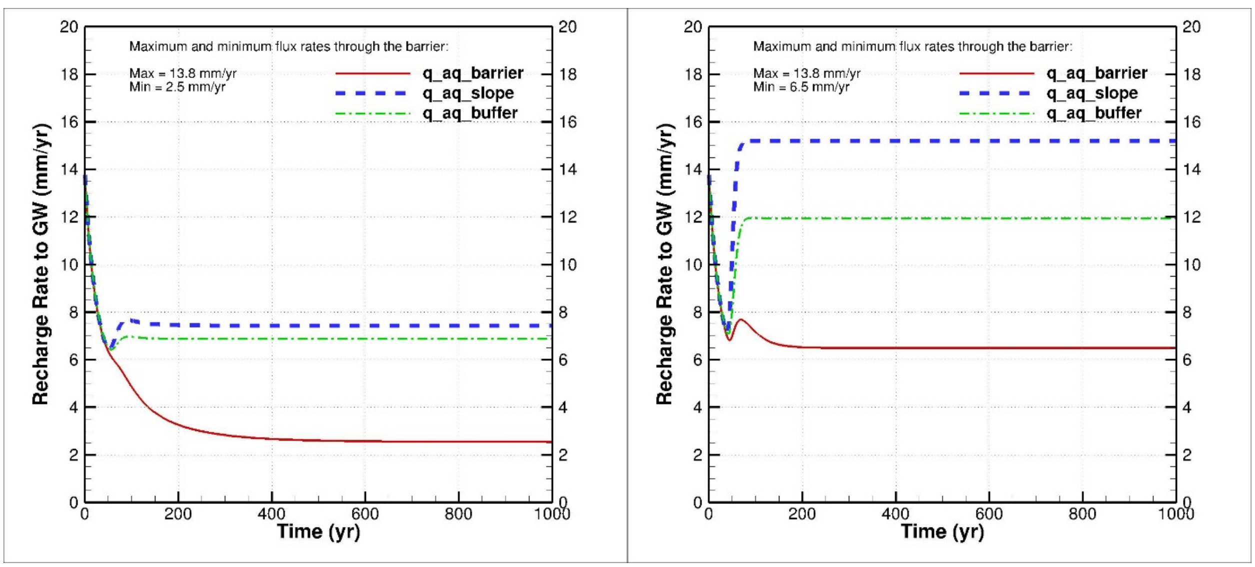

(c) Case 2 (Average surface barrier) (d) Case 3 (Poor surface barrier)

Figure B.2. Time course of the aqueous flux rate to the groundwater. The horizontal axis is the time since barrier deployment in 2020.

B.3 Distribution of Contaminants

The distributions of contaminants 100 years after surface barrier deployment are shown in Figure B.3, Figure B.4, and Figure B.5 for NO_3, Tc-99, and U-total, respectively. The mass per unit depths (MPD) from 2020 to 2120 are shown in Figure B.6, Figure B.7, and Figure B.8 for NO_3, Tc-99, and U-total, respectively. The difference among the four simulation cases were so small that they cannot be distinguished visually. Examples of the processed eSTOMP results comparing solute mass distributions across cases at 100, 500, and 1,000 years are shown in the main text in in Figure 7, Figure 8, and Figure 9.

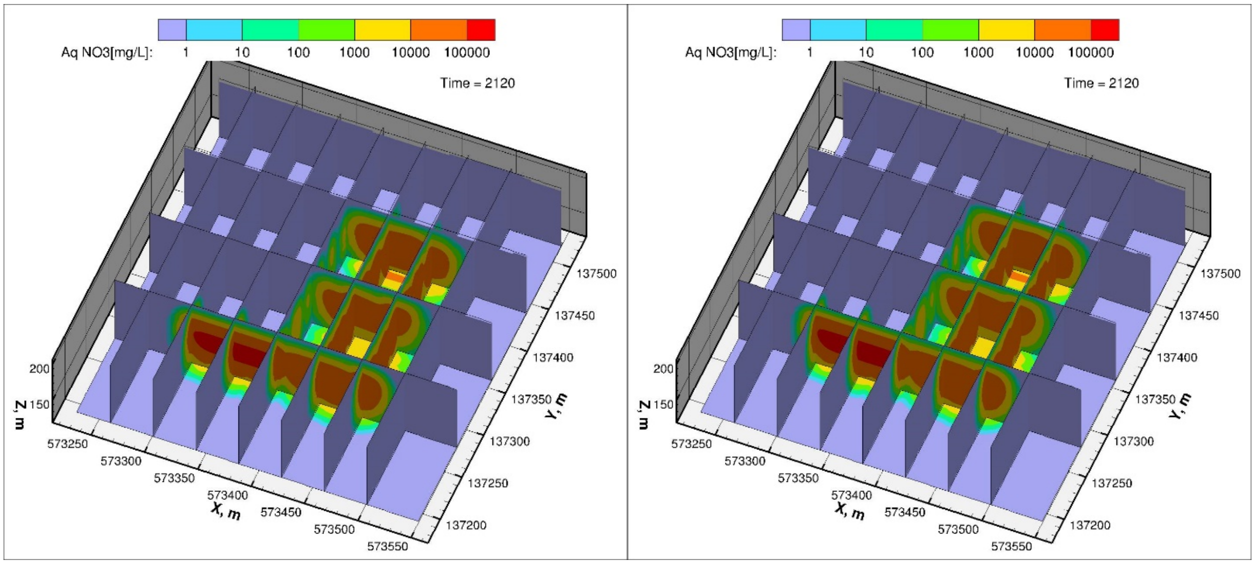

(a) Case 0 (No surface barrier)

(b) Case 1 (Good surface barrier)

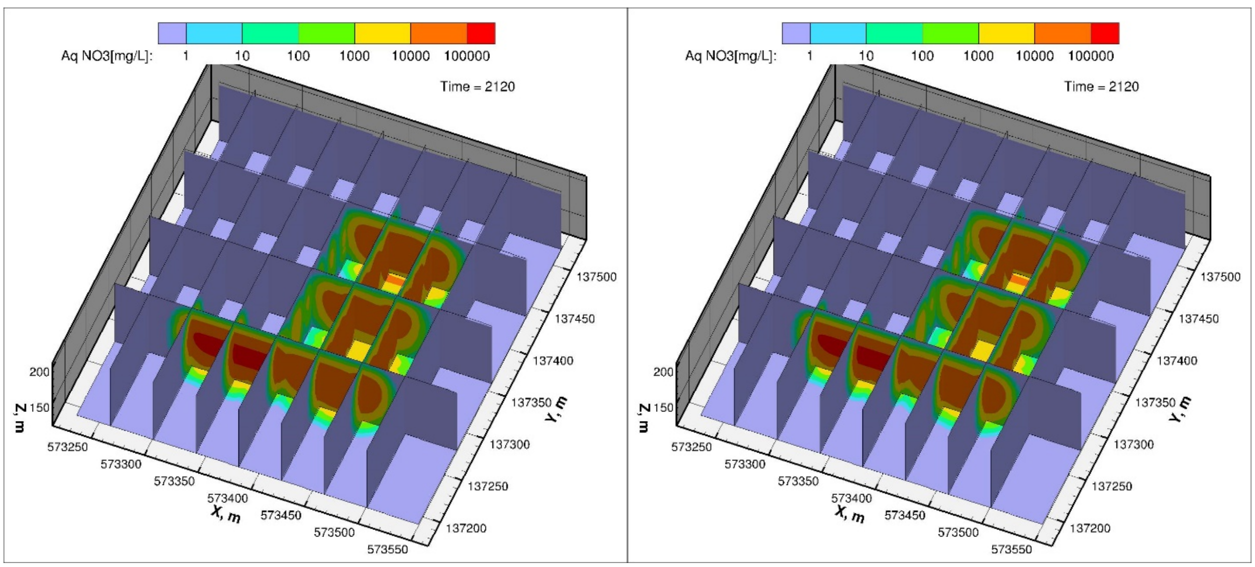

(c) Case 2 (Average surface barrier)

(d) Case 3 (Poor surface barrier)

Figure B.3. Aqueous concentration of NO_3 at 2120, 100 years after surface barrier deployment.

Generally, the MPD for Case 0 is similar to the MPD for Case 4, while the MPDs for Cases 2 and 3 are similar to each other. This is due to the recharge rates from the ET barrier – Cases 0 and 4 had the same value of 3.0 mm yr^{-1}, while Cases 2 and 3 had more similar values (0 and 0.5 mm yr^{-1}). The results indicate that the reduction from 3.0 mm yr^{-1} to zero had only relatively small effect in slowing down contaminant migration.

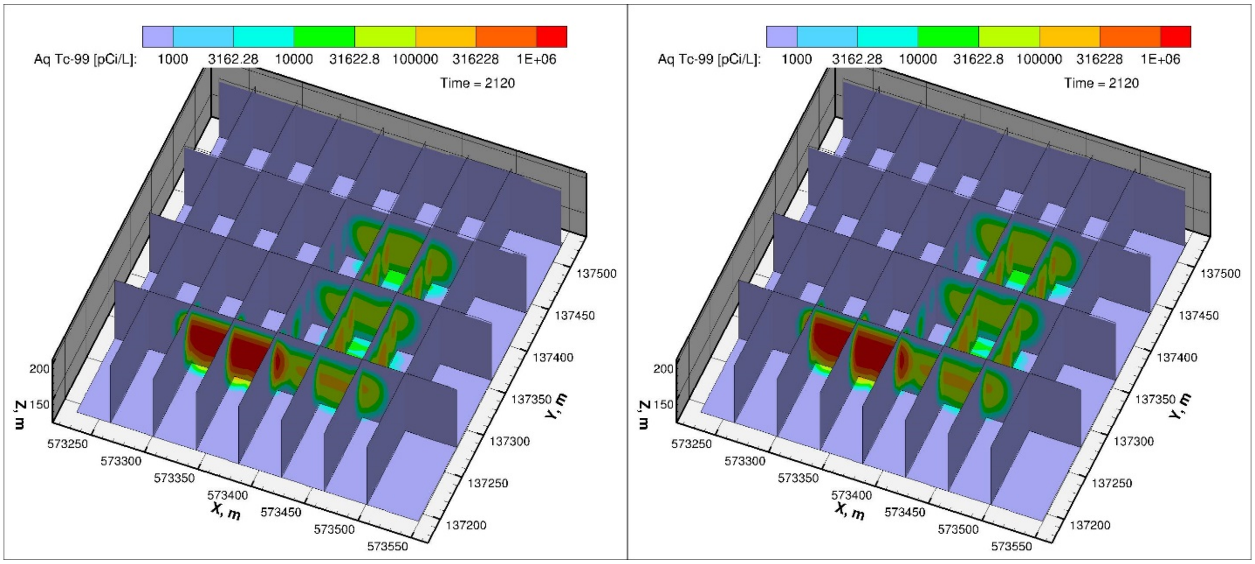

(a) Case 0 (No surface barrier) (b) Case 1 (Good surface barrier)

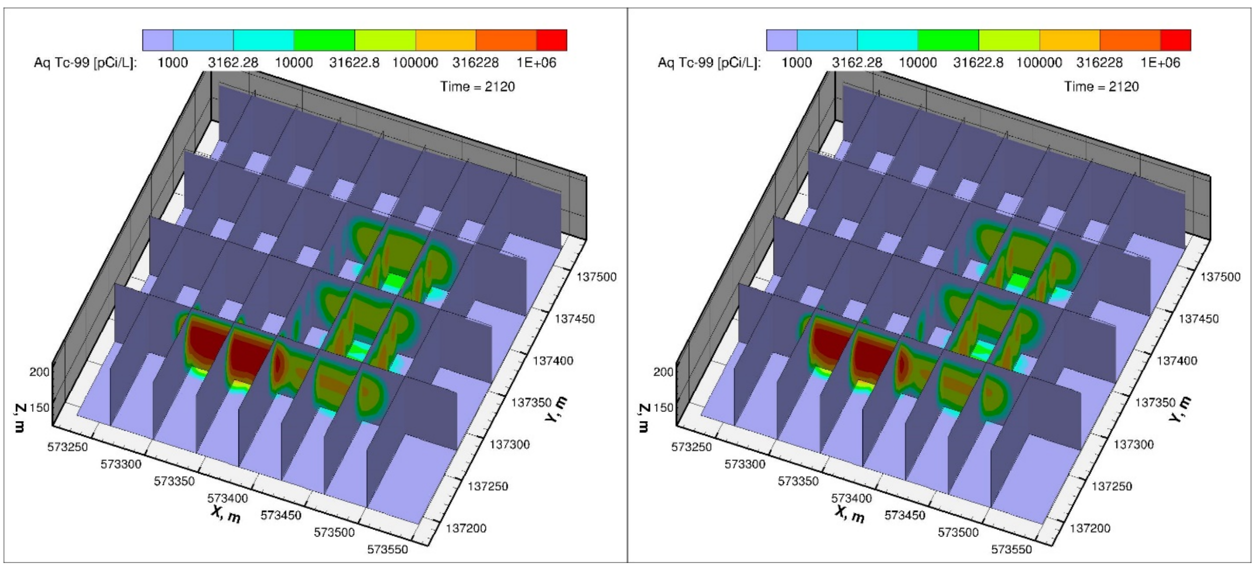

(c) Case 2 (Average surface barrier) (d) Case 3 (Poor surface barrier)

Figure B.4. Aqueous concentration of Tc-99 at 2120, 100 years after surface barrier deployment.

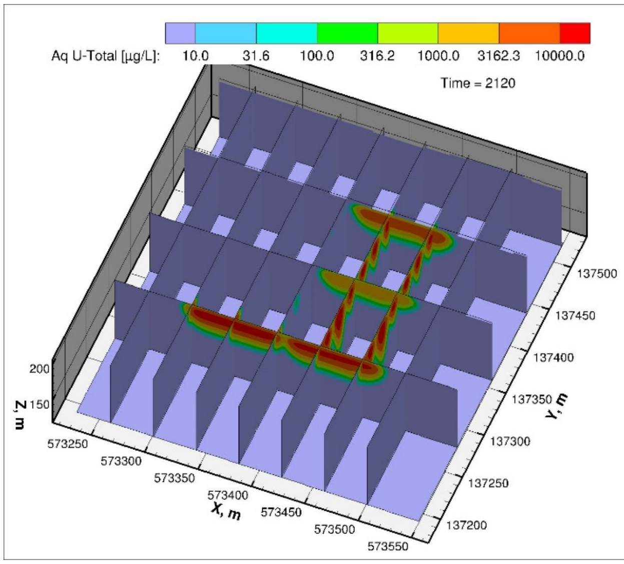

(a) Case 0 (No surface barrier)

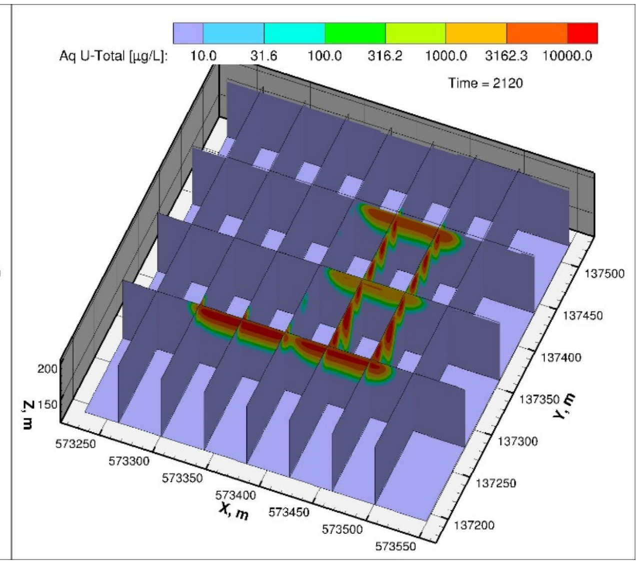

(b) Case 1 (Good surface barrier)

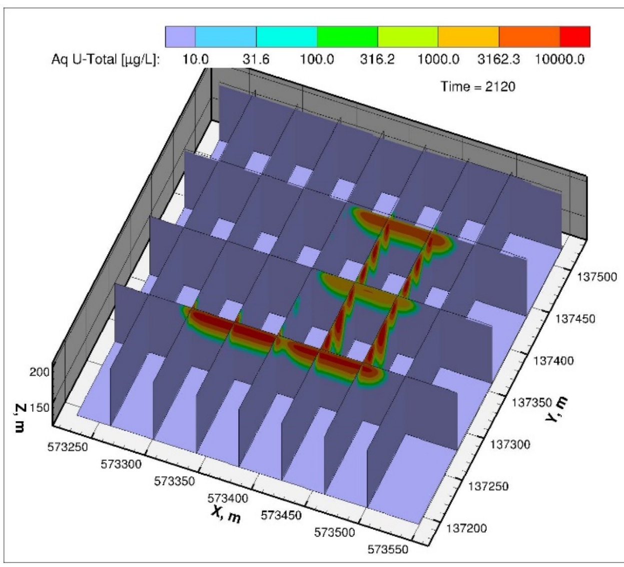

(c) Case 2 (Average surface barrier)

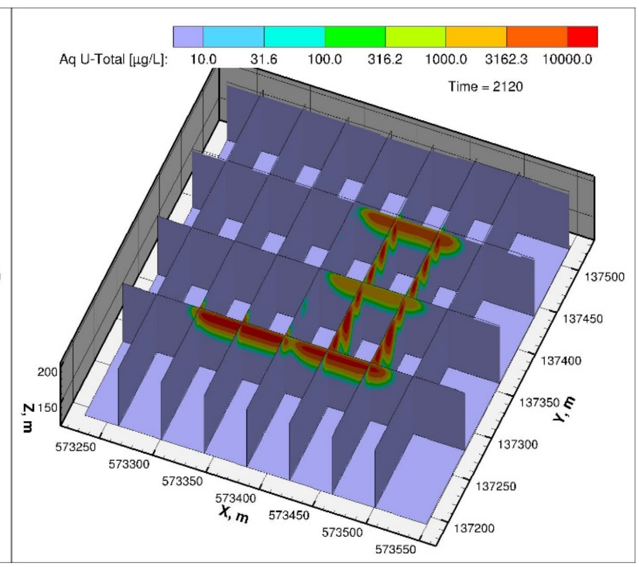

(d) Case 3 (Poor surface barrier)

Figure B.5. Aqueous concentration of uranium at 2120, 100 years after surface barrier deployment.

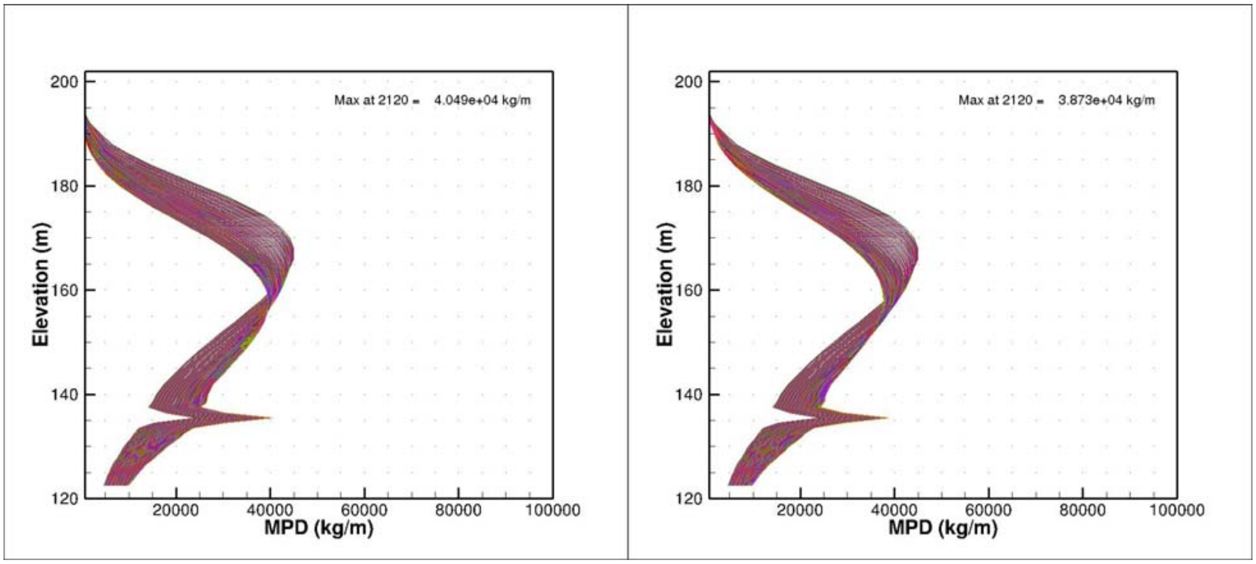

(a) Case 0 (No surface barrier) (b) Case 1 (Good surface barrier)

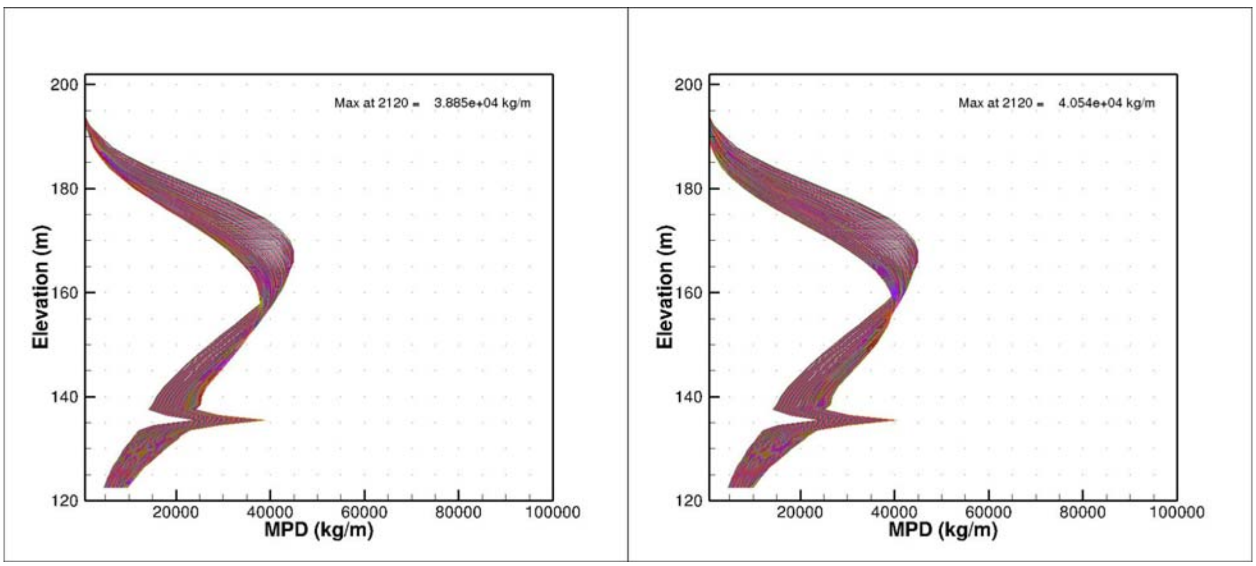

(c) Case 2 (Average surface barrier) (d) Case 3 (Poor surface barrier)

Figure B.6. Mass per unit depth for NO_3 (kg/m). Each plot consists of 101 lines corresponding to the time from year 2020 (the upper-most line) to 2120 (the lower-most line) at 1-year intervals.

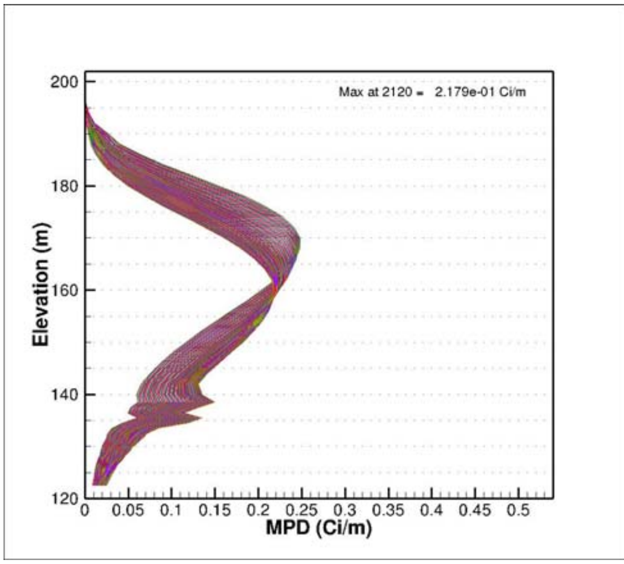

(a) Case 0 (No surface barrier)

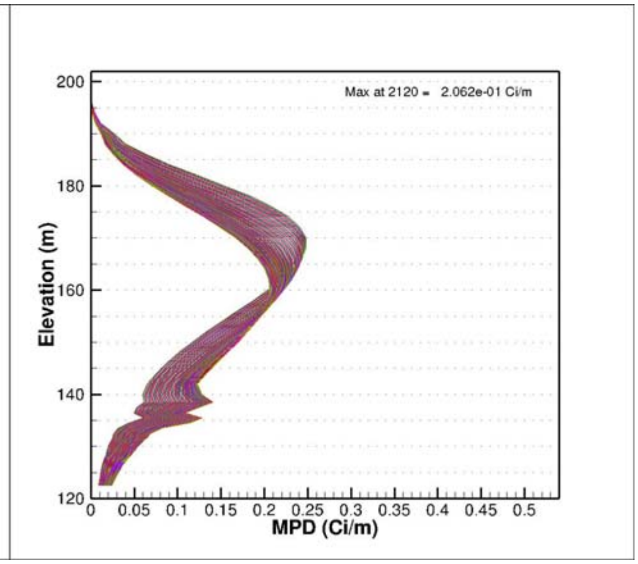

(b) Case 1 (Good surface barrier)

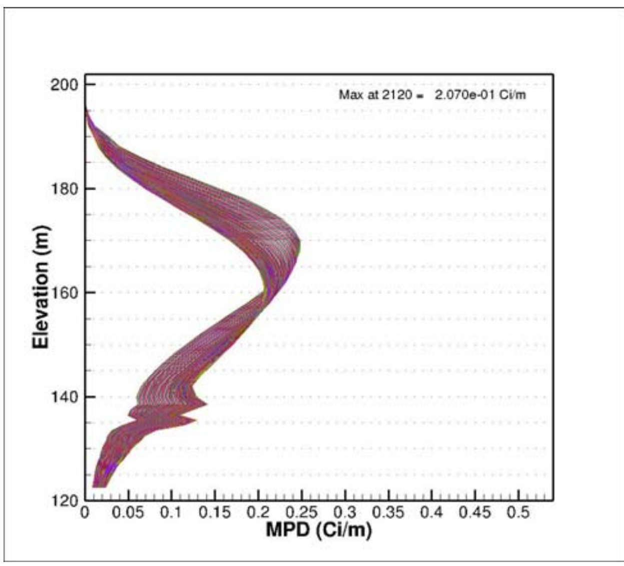

(c) Case 2 (Average surface barrier)

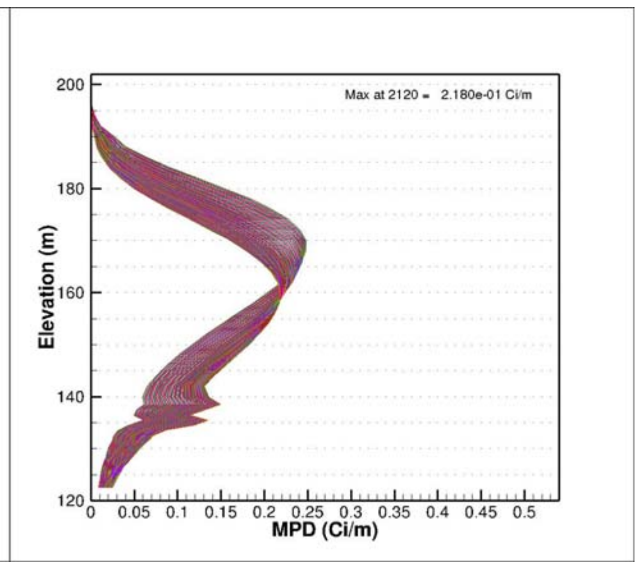

(d) Case 3 (Poor surface barrier)

Figure B.7. Mass per unit depth for Tc-99 (Ci/m). Each plot consists of 101 lines corresponding to the time from year 2020 (the upper-most line) to 2120 (the lower-most line) at 1-year intervals.

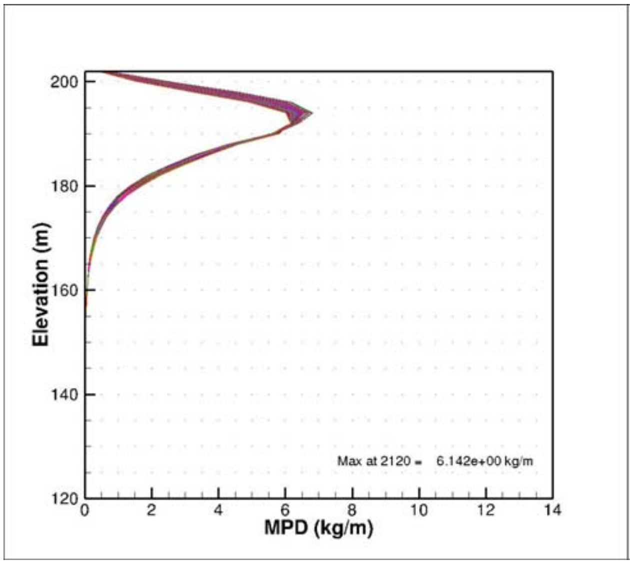

(a) Case 0 (No surface barrier)

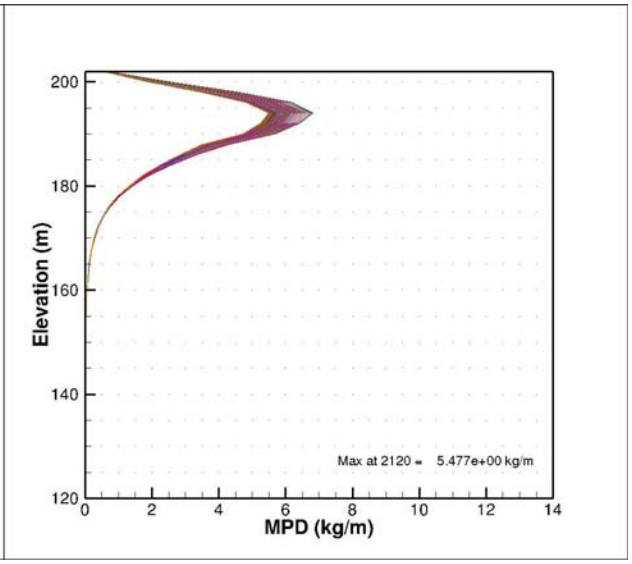

(b) Case 1 (Good surface barrier)

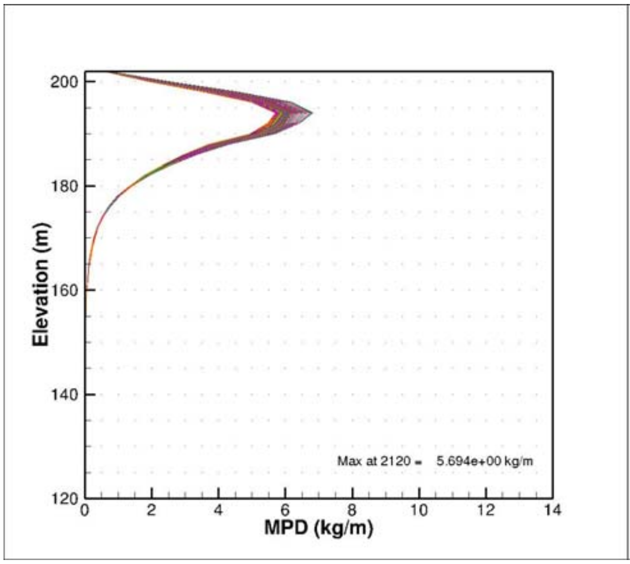

(c) Case 2 (Average surface barrier)

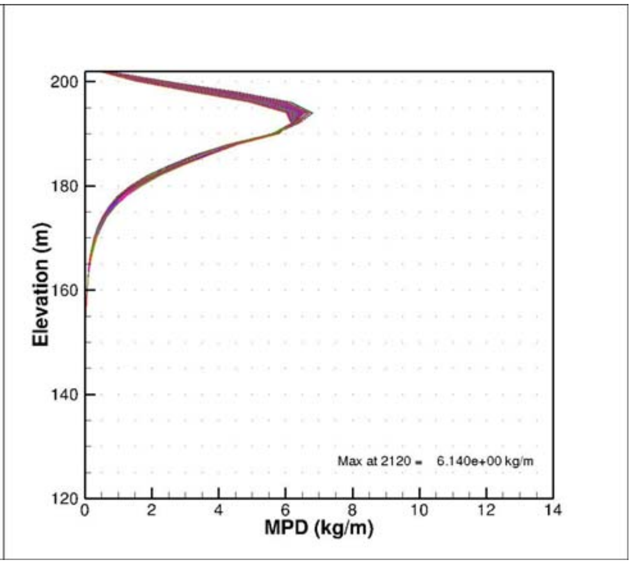

(d) Case 3 (Poor surface barrier)

Figure B.8. Mass per unit depth for uranium (kg/m). Each plot consists of 101 lines corresponding to the time from year 2020 (the upper-most line) to 2120 (the lower-most line) at 1-year intervals.

B.4 Horizontal Extents of Contaminant Plumes

The shapes and extents for NO_3, Tc-99, and U-total are shown in Figure B.9, Figure B.10, and Figure B.11, respectively, from 2020 to 2120. For any of the contaminants, neither the shape nor the size of any of the plumes had noticeable changes over the period of 100 year after surface barrier deployment. Figure B.12 compares the plume extent of the same contaminant for the four cases. Again, the differences are very small. This indicates negligible lateral migration of contaminants. The reason could be the sufficiently large ET barrier rather than the actual plumes (Figure 5). Another reason is the dilution of recharging water near the boundary of the plumes. Once the contaminant concentration is less than the MCL, it is not considered as part of the plume anymore.

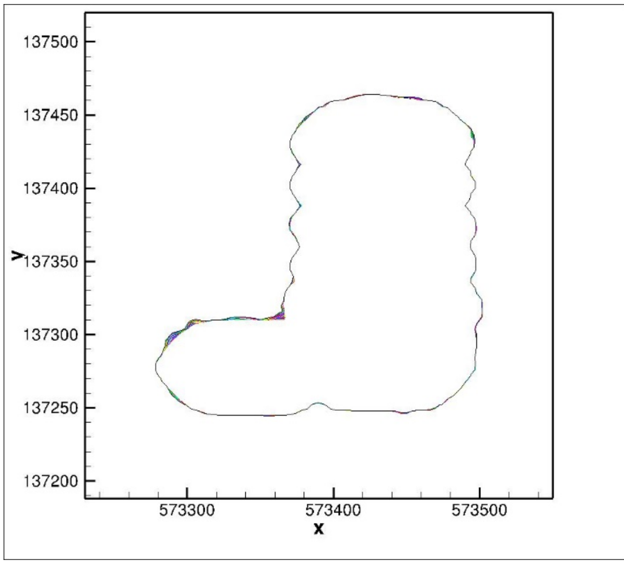

(a) Case 0 (No surface barrier)

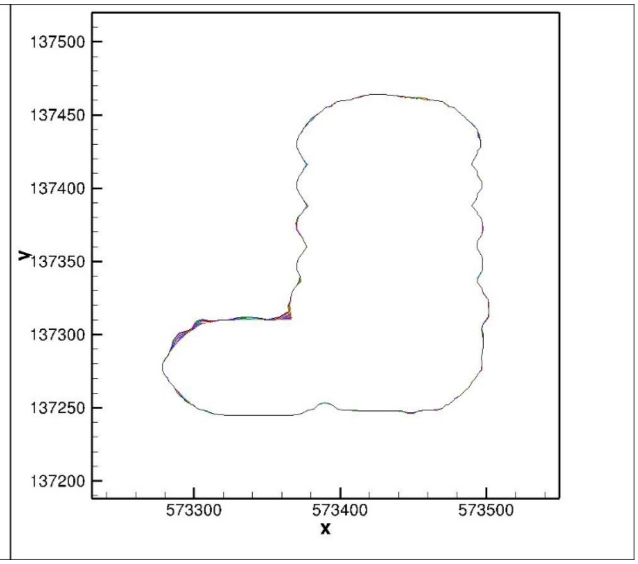

(b) Case 1 (Good surface barrier)

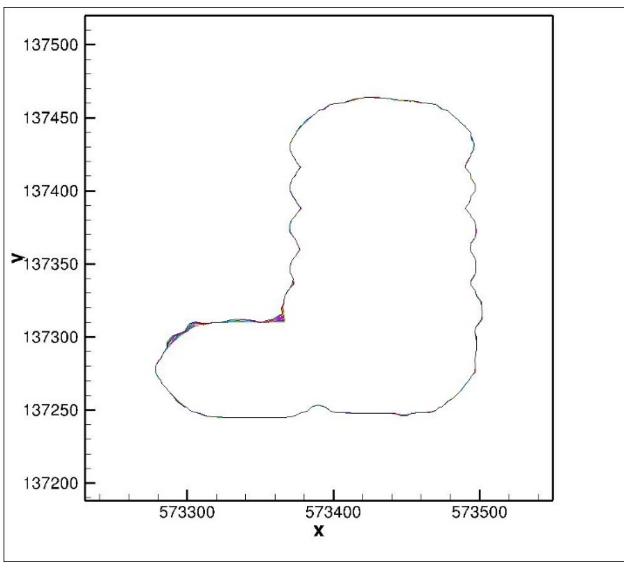

(c) Case 2 (Average surface barrier)

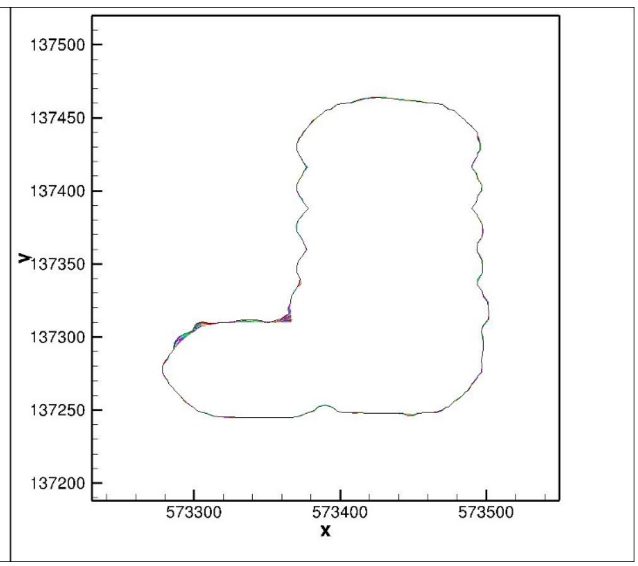

(d) Case 3 (Poor surface barrier)

Figure B.9. NO_3 plumes projected on a horizontal plane. Each plot consists of 101 lines corresponding to the time from year 2020 to 2120 at 1-year intervals.

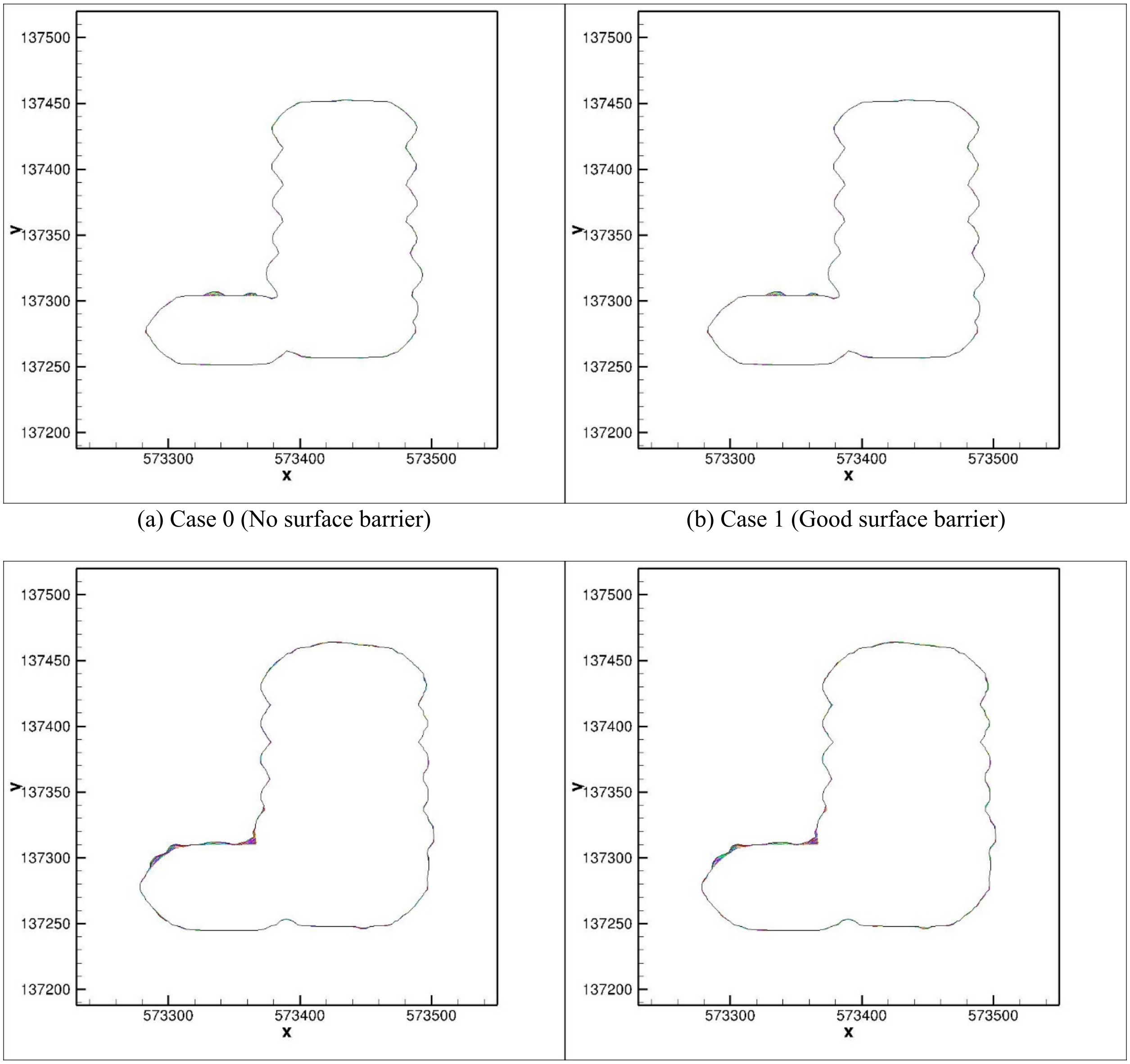

(a) Case 0 (No surface barrier)

(b) Case 1 (Good surface barrier)

(c) Case 2 (Average surface barrier)

(d) Case 3 (Poor surface barrier)

Figure B.10. Tc-99 plumes projected on a horizontal plane. Each plot consists of 101 lines corresponding to the time from year 2020 to 2120 at 1-year intervals.

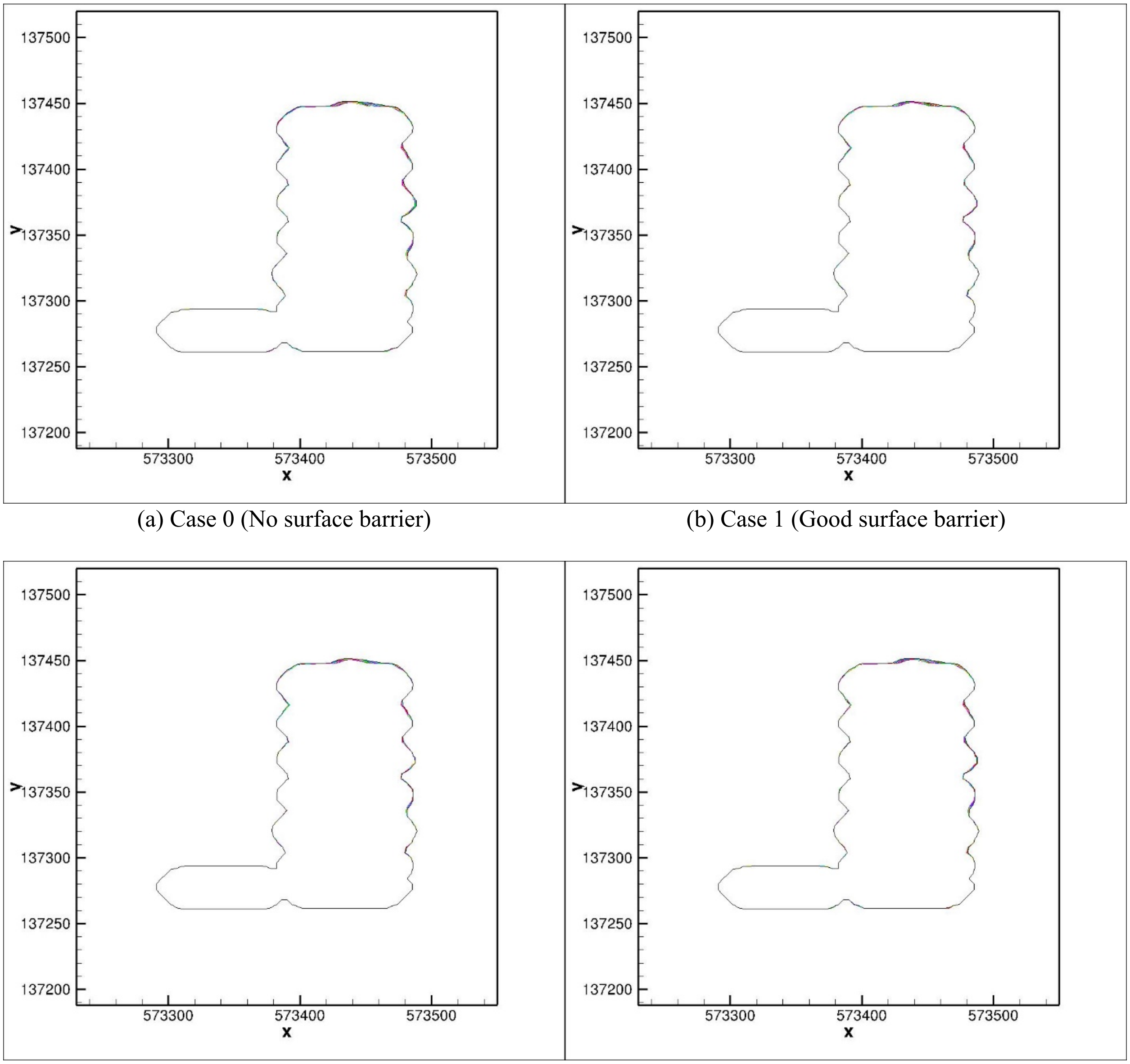

(a) Case 0 (No surface barrier)

(b) Case 1 (Good surface barrier)

(c) Case 2 (Average surface barrier)

(d) Case 3 (Poor surface barrier)

Figure B.11. Uranium plumes projected on a horizontal plane. Each plot consists of 101 lines corresponding to the time from year 2020 to 2120 at 1-year intervals.

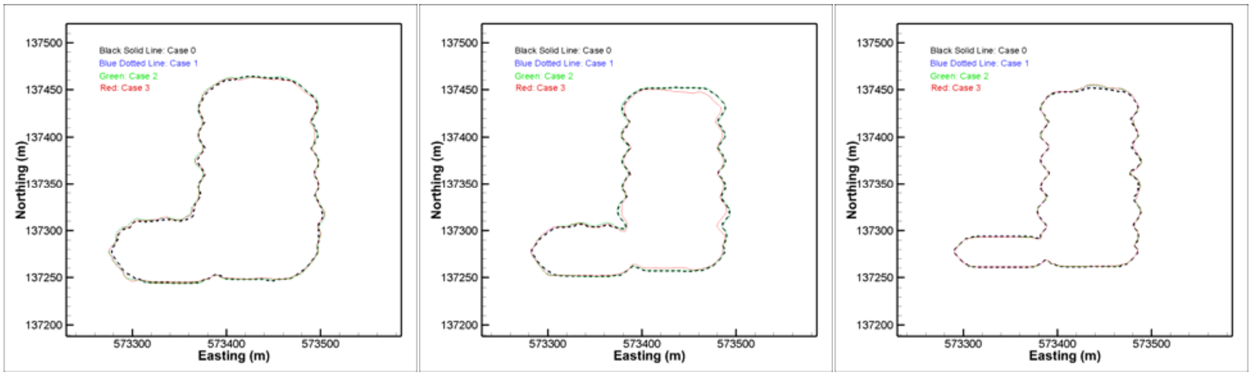

Figure B.12. Contaminant plumes projected on a horizontal plane in 2120.

B.5 Contaminant Flux at Groundwater Table

The contaminant flux is shown in Figure B.13 for NO_3, Figure B.14 for Tc-99, and Figure B.15 for U-total. For all the cases, zero contaminant flux rate was simulated below the side slope and the buffer zone, meaning no contaminants had migrated far enough laterally to reach these zones. For all contaminants, the results for Case 0 were similar to those for Case 3 while results for Case 1 were similar to those for Case 2, suggesting that drainage through the side slope was not strongly correlated to contaminant transport rates for this example. The contaminant flux to groundwater was less when a better surface barrier was deployed.

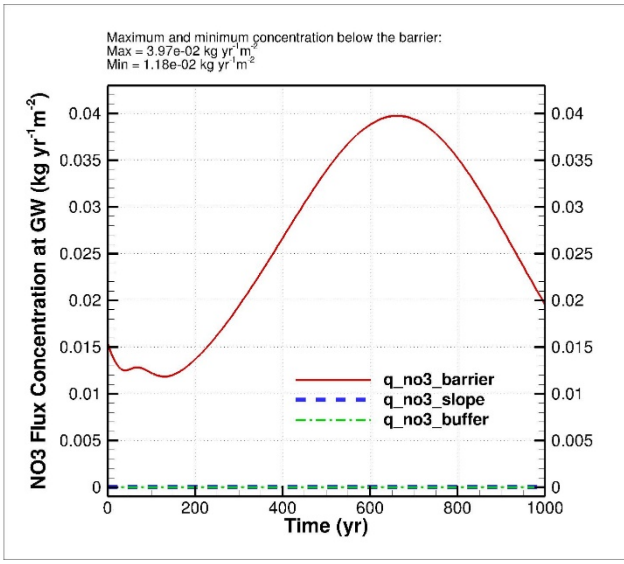

(a) Case 0 (No surface barrier)

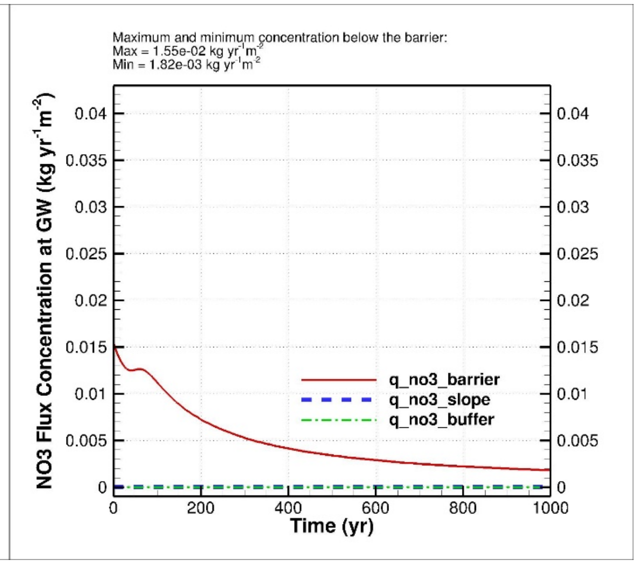

(b) Case 1 (Good surface barrier)

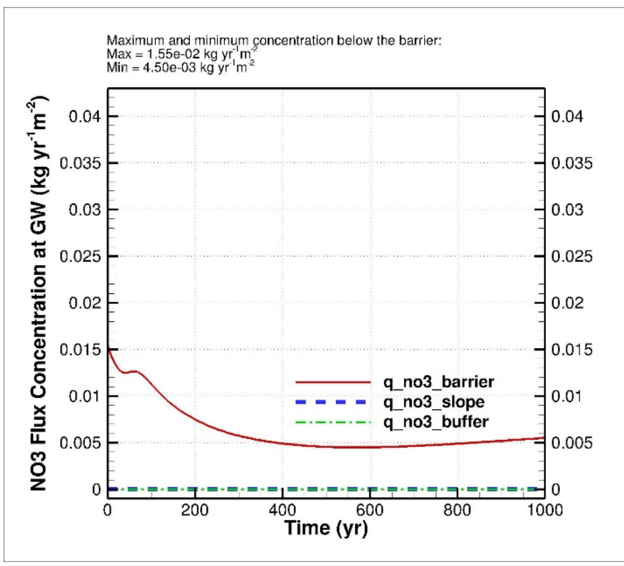

(c) Case 2 (Average surface barrier)

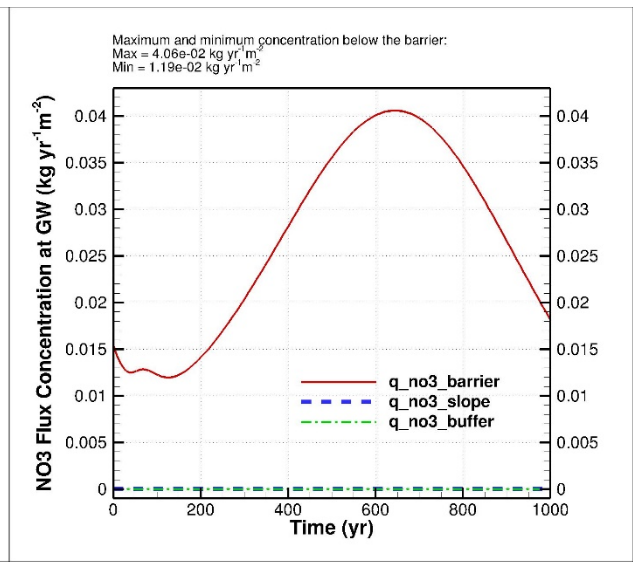

(d) Case 3 (Poor surface barrier)

Figure B.13. Time course of the NO_3 concentration at the groundwater table.

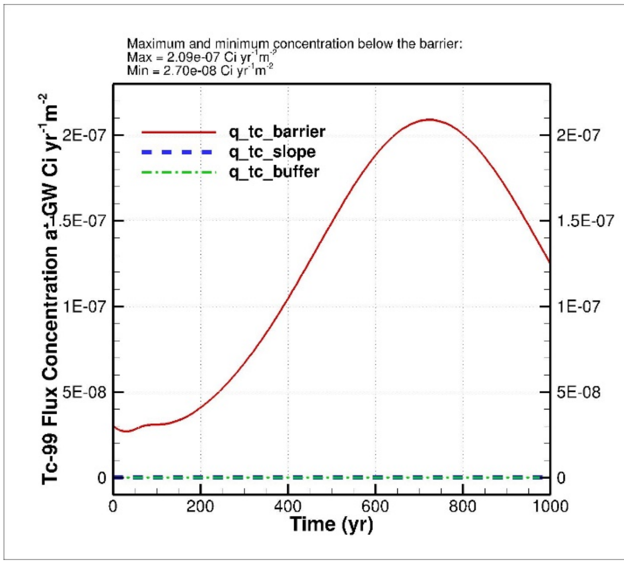

(a) Case 0 (No surface barrier)

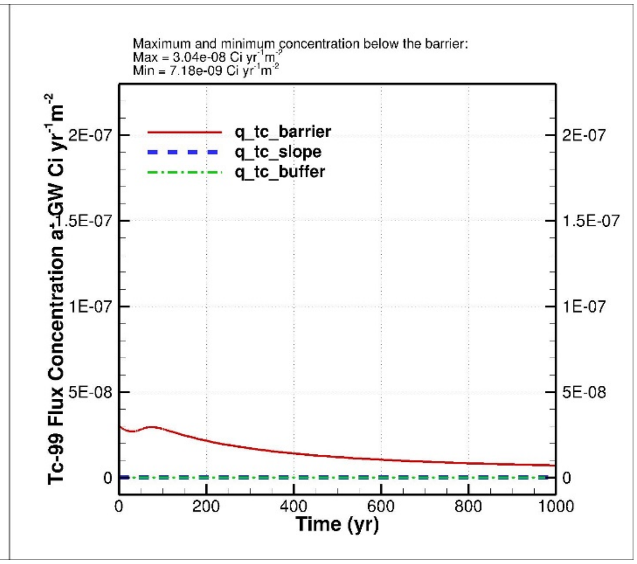

(b) Case 1 (Good surface barrier)

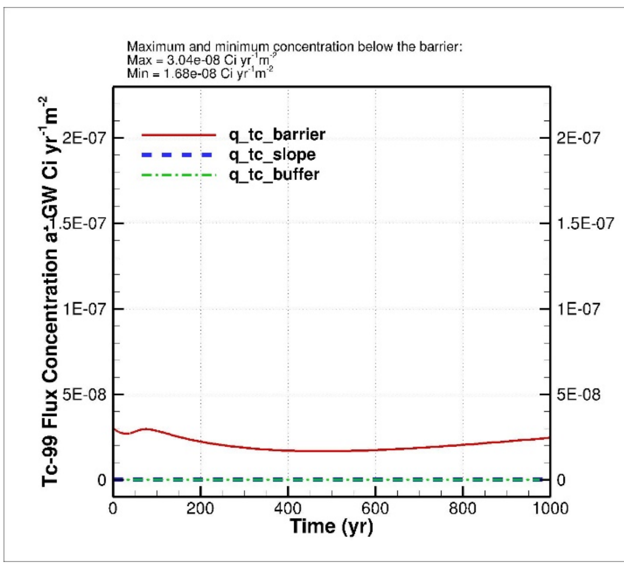

(c) Case 2 (Average surface barrier)

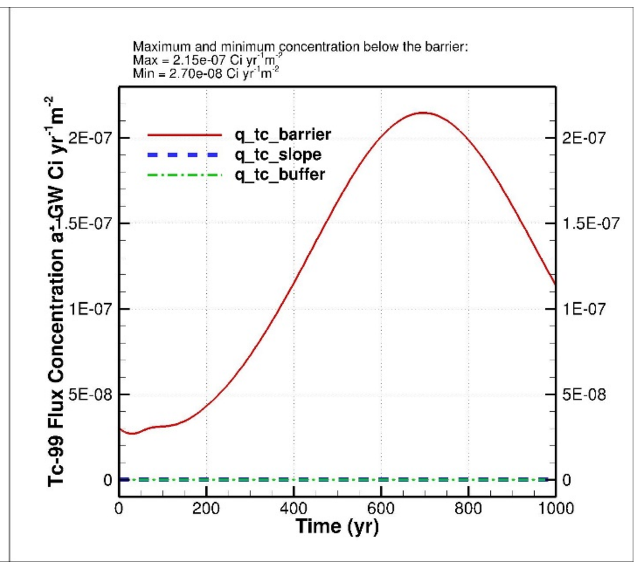

(d) Case 3 (Poor surface barrier)

Figure B.14. Time course of the Tc-99 concentration at the groundwater table.

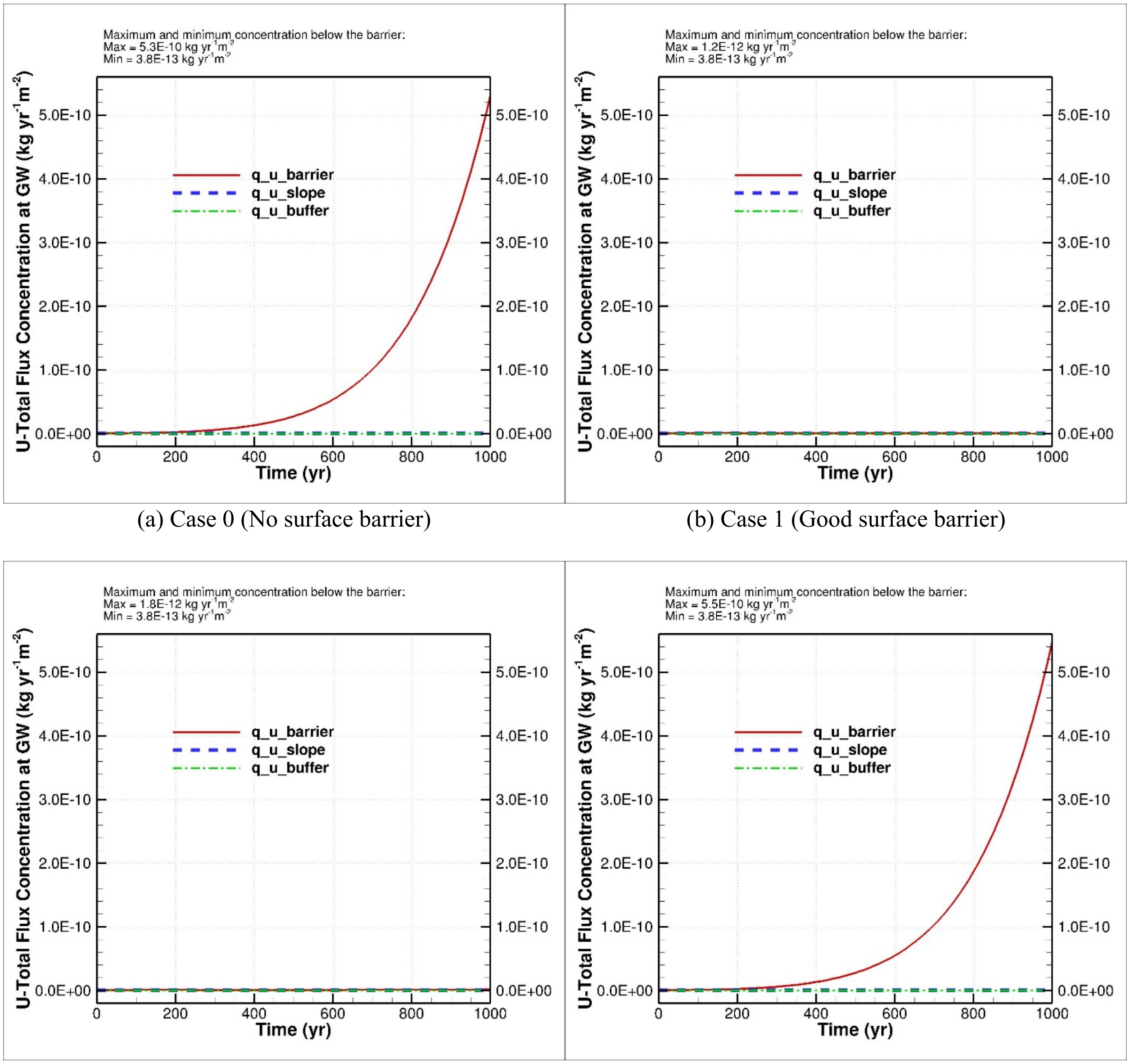

(a) Case 0 (No surface barrier)

(b) Case 1 (Good surface barrier)

(c) Case 2 (Average surface barrier)

(d) Case 3 (Poor surface barrier)

Figure B.15. Time course of the uranium concentration at the groundwater table.

PNNL-29186
DVZ-RPT-0027 Rev 0.0

Pacific Northwest National Laboratory

902 Battelle Boulevard
P.O. Box 999
Richland, WA 99354
1-888-375-PNNL (7665)

www.pnnl.gov